Dear Editor,

According to the reviewers' comments and suggestion, we have made revision to our manuscript. These main changes are given as follows:

1) We give more detailed descriptions about the methodology to better understand the global assimilation in $1^o \times 1^o$ grid resolution.

2) According to the comment about initial concentration field by reviewer #1, we discard the result of the first year 2000, and all of the analysis is updated according to the results from 2001 to 2007.

3) According to the comment by reviewer #1, we added the discussion about the relationship with geostatistical methods led by Michalak et al. (2004).

4) We give more details and explanation about the parameter settings in the application.

The point-by-point response to the reviews and the detailed changes are listed in the attachments.

Great thanks to you and the referees for the time and effort you expend on this paper.

Best Regards.

Sincerely yours,

Yong Li

Response to Referee #1

We would like to thank referee #1 Rayner Peter for his comprehensive review and detailed suggestions concerning our manuscript. Those comments are all valuable and very helpful for revising and improving our paper. We have studied these comments carefully and made the suggested revisions. Our response to the reviewer's comments is given below.

General comments:

Comment: This paper presents an optimization of 8 years of CO_2 fluxes from the terrestrial biosphere and ocean using a method the authors describe as a dual optimization. I am still a bit unclear on several methodological details of the paper so some of what I'm going to say in the following review is probably wrong. The authors should take notice of my misunderstandings though because they indicate places where the paper should be clearer. The most striking example of this is the elements in the control vector of the optimization. I think this vector contains a series of multipliers (λ) for patterns of terrestrial and ocean fluxes plus one global offset which is used to adjust the atmospheric concentration. The atmospheric concentration is adjusted once per assimilation window (six weeks) but I am unclear about the time resolution of λ. If it is also six weeks then the method seems to be an ensemble version of a classic synthesis inversion (e.g. Enting et al., 1995; Rayner et al., 1999)) with the time windowing technique suggested by Law (2004). If this is correct then some of the claimed advantages of the method don't apply. For example, the authors claim (P14291) that the 1x1 degree resolution of the model avoids the aggregation problem described by Kaminski et al. (2001). In fact the aggregation problem concerns flux patterns in the real world which are outside the subspace spanned by the control vector. The resolution of the flux patterns themselves (i.e. the transport model) doesn't help this problem.

Response: Thank you for these comments. For the time resolution of λ, we actually use a similar strategy to that in Peters et al., (2005). The weekly multiplier at each time *t* in this study is estimated six times and the final result is used as the estimates of λ_t. We have added these descriptions in Sec 2.2 and Sec 2.3 (see lines 27-32, page 6 and lines 17-18, page 8 for details).

Moreover, the method in this study is different from an ensemble version of a classic synthesis inversion from two main aspects. Firstly, we use a newly proposed method DOM (Dual Optimization Method, Zheng et al., 2014) to estimate the multipliers (λ) and gridded flux simultaneously in each window instead of using the classical Bayesian synthesis method. In a classical synthesis inversion method, researchers either use the Bayesian Synthesis Inversion Method (shorted for BSIM in my manuscript) to estimate the flux only (e.g. Enting et al., 1995) or use an ensemble version to estimate multipliers (e.g. Peters et al., 2007). The DOM uses the information of CO_2 concentration observations to obtain the optimized multipliers and fluxes simultaneously based on a statistical model (See Zheng et al., 2014 for the details). Secondly, the previous ensemble method usually involves a forecast model for multipliers (e.g. Lokupitiya et al., 2008, Peters et al., 2007, 2010). This is different from our system

which does not need a forecast model for the multipliers.

For the aggregation error, we agree that the aggregation problem concerns the internal shape of the flux pattern. But GCAS-DOM can still show its superiority. Kaminski et al., (2001) pointed that the aggregation errors for large regions may be of the same order of magnitude as the fluxes themselves and hence inverted fluxes should be cautiously used when answering practical issues. On the other hand, a global inversion in fine grids with long periods based on a batch synthesis inversion method may often be computationally prohibitive. GCAS-DOM incorporates a moving-window method to do global assimilation in a high-resolution grid, and therefore it would significantly advance our understanding of regional carbon cycles. We have deleted the sentence "... avoids the aggregation problem " and rewritten it as follow:

" ...The $1^o \times 1^o$ revolution for flux estimation at the global scale in our study is higher than those in previous studies and therefore it would significantly advance our understanding of regional carbon cycles."

For details, please refer to lines 5-7, page 17.

Comment: I also don't quite understand the computational burden of the problem. As I understand it, the authors solve for approximately 250 fluxes each six week window (weeks here defined like GlobalView with 48 weeks in a year). That's about 2000 unknowns per year or approximately 16000 for the whole period. That's not an immense problem even using the analytic matrix methods. There might be other reasons for the windowing technique, e.g. an effective weak constraint on transport but I don't accept the primary reason is computational.

Response: Thank you for the comment. In fact, the computational amount of the system depends on two aspects: the number of multipliers and fluxes. For each six week window, we solve for about 250 multipliers. However, the resolution of flux is 1 degree, which generates 64800(180*360) elements each week. Therefore, the computational burden mainly depends on the dimension of the flux rather than the multipliers. That's about 3,130,400 (64800*48) unknowns per year and the relevant cost of matrix operations (see Eq. (12)) will be at least $3{,}130{,}400^2$ which is an immense problem. We have added this explanation in the revised manuscript (see lines 8-11, page 6).

Comment: Of course it's possible I'm completely misunderstanding the approach. The authors may solve for large-scale patterns plus deviations from these, in the spirit of the geostatistical methods pioneered by Michalak and colleagues. If so, please disregard the above but the authors should discuss the relationship with these techniques.

Response: Thank you for the suggestion. We solve for global-scale patterns plus the optimization of model parameters. We have added the discussion about the relationship with geostatistical methods led by Michalak et al. (2004) in the revised paper (see lines 26-30, page 2 and lines 9-11, page 3).

Comment: another concern is independent of the flux resolution and concerns the treatment of

the initial condition for each window. Quite reasonably, the prior estimate for this is the result of the simulation of the previous window. The concentration is then corrected by a global offset to minimise the difference with surface values at the end of the window. This updated concentration distribution is used, without correction, as the initial condition for the next window. I see three problems with this:

1. The adjustment to match concentrations introduces a change of CO_2 mass in the atmosphere that is not associated with any fluxes. If this correction has a consistent sign it will lead to a flux series that is inconsistent with the change of CO_2 concentration over the whole timeseries, the aspect of atmospheric CO_2 of which we are most sure.

2. Why correct only the mean concentration? Peylin et al. (2005)) showed a method for improving those aspects of the 3-dimensional concentration distribution observable by the concentration measurement network.

Response to problems 1 and 2: Thank you for these comments. There may be some misunderstanding about the treatment of the concentrations for each window. In fact, we not only update the concentrations based on its 3-dimensional distribution, but also added an extra correction according to the mean of observations in situ. These can be described as follows. In a classic batch inversion, the measurement M could be explicitly expressed as (Peylin et al., 2005):

$$\mathrm{M} = \mathrm{H}_0 \mathrm{C}_{|\mathrm{t}_0} + \mathrm{H}_s \, \mathrm{S}$$

where $\mathrm{C}_{|\mathrm{t}_0}$ represents the initial condition and S represents the unknown sources during the study period. Now suppose that we have obtained the optimized flux at time *t*, $\hat{s}_t$, and aim to estimate the fluxes at time *t*+1, s_{t+1}. In an assimilation system, the initial condition in the current window includes the impacts not only from the initial condition but also from fluxes before time *t*+1 , which is denoted as *C*(t) (See Fig 1). Naturally, we run the transport model using the previously stored quantities *C*(t-1) forced by the optimized fluxes $\hat{s}_t$ to get a 3-dimensional distribution of *C*(t). A previous assimilation system e.g. Peters et al., (2005) just used the above 3-dimensional distribution as the initial condition for the window. In this study, we hold the opinion that the spatial pattern of optimized flux $\hat{s}_t$ is rational and therefore can be used to simulate the *C*(t). However, the comparison between simulated and observed concentrations indicates that there exists a systematic error in the simulated concentration. So we add an adjustment of the average for the 3-D concentration to correct this error but keep the same spatial pattern of the 3-D concentration.

Nevertheless, this extra correction only use the average information as the referee said. We have to admit it is a simple strategy but has good effects. To test these effects, we run the system under the same configuration but without the extra correction (similar to that by Peters et al., 2005). The initial concentration prescribed here is set as the site averaged concentration in the last week of 1999 (see lines 5-6, page 9). The following figure compares the total annual fluxes of the globe for the two measures with and without extra correction. The system without this correction generates a -8.931 Pg C/year carbon budget for the first year 2000 which may be strongly impacted by the initial concentration, while the system with this correction quickly stabilizes and produces a relatively reasonable annual carbon budget for the spin-up period. The difference of total carbon budget between the two measures diminishes in 2002. Further research on the system bias would be done in a following paper.

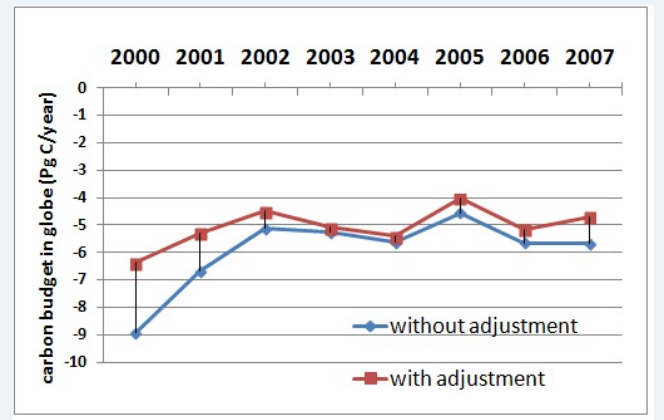

Figure: The total annual fluxes in globe for with and without extra correction

Comment: **3**. No account seems to be taken of uncertainty in the initial concentration field when calculating fluxes. This is a pretty direct consequence of leaving the 3-d concentration out of the state vector. Peylin et al. (2005) also showed that errors in the initial field could affect the model-measurement mismatch for 20 days i.e. about half the assimilation window so it would seem to be important to deal with this.

Response: Thank you for the comment. We agree that the error in initial concentration field can affect the mismatch for a relatively short time (about 20 days). Therefore, the assimilation system usually needs a spin-up period. We have added this description in the revision (lines 3-5, page 9). Normally, we suggest discarding the estimates of the first one to two years in the data assimilation period (Nassar et al., 2011; Deng et al., 2011; Jiang et al., 2013). In our study, we have performed several tests by using different initial concentration values and the results showed that the optimized values after 1 year is reliable and hardly impacted by the initial concentration field. We use a globally-uniform 3-D CO_2 field of site-averaged concentration in the last week of 1999 as the initial concentration of the system and the results from 2001 to 2007 are reasonably used for analysis. We have discarded the results in 2000 in the revised paper and all of the analysis is based on the results from 2001 to 2007. Figs 4-14 and Tables 2-4 have been updated and the average value is computed based on the results of 2001-2007.

Comment: I also question the use of multipliers for flux patterns themselves rather than the more conventional use of separate multipliers for GPP and respiration. The problem arises from the diurnal cycle. I'm not clear whether the authors retain the diurnal cycle of fluxes from BEPS. If they do then a change of sign of the flux will also change the sign of the diurnal cycle. Since many of the observations in GLOBALVIEW represent particular times of the day this could affect the model-data mismatch at the heart of the inversion.

Response: Thank you for the comment. In fact, we tried to estimate multipliers for GPP and ER, separately. As both ER and GPP are much larger than the NEP fluxes by approximately

one order of magnitude, they are sensitive to multipliers. Moreover, the strong correlation between ER and GPP could result in poor performance in stability. Therefore, we decided to adjust the outcome of their differences rather than their separate influences (see lines 27-30, page 4). Moreover, we use the weekly average fluxes from BEPS and corresponding concentration in situ at weekly interval to avoid the problems of the diurnal cycle (we have added this statement in lines 13-14, page 9). In addition, the multipliers are constrained to be greater than zero by the uncertainties on the λ parameters and hence they would not change the sign of the flux. We have added this explanation in the revised paper (see line 30, page 9).

Comment: My other general concern is prior uncertainties. These are handled via uncertainties on the λ parameters. If I understand correctly these are set at 0.1% for regions outside China and 1% for China. These uncertainties are not arbitrary, they should represent the statistics of differences between simulations of the model used for the prior and the true fluxes. See Chevallier et al. (2006, 2012) for details on how they can be calculated and some indicative numbers from a different model. The uncertainties used in this study seem very low. For example they approach 0 in the transition season as the net flux approaches 0 although the uncertainty should not. This has consequences for the results. The relatively small changes in λ are a likely consequence of these very small uncertainties. I suggest this choice should be justified.

Response: Thank you for these comments. This issue is a key problem in GCAS-DOM. The constrained variance for parameters (line 17, page 7) is used to obtain an unique solution for λ, rather than to determine the prior uncertainties of fluxes. The prior uncertainty used in this study is the model error matrix Q for the prior flux (line 8, page 5). As we described in our manuscript (lines 10-12, page 13), we use uncertainties of 1.98 Pg C/year and 0.93 Pg C/year for the land and oceanic fluxes, respectively, which are not low compared to previous studies (e.g. Deng et a.,2007, 2011, Gurney et al.,2003,2004).

On the other hand, the flux in a grid consists of six components for different PFTs and the similar climate condition in a grid will lead to strong correlation of these components. So we propose an adaptive version of DOM by adding additional regularization of parameters (lines 10-17, page 7). For the range of λ, we think that the value should be around 1 and set an initial interval of [0.7, 1.3], as the preferences of BEPS are basically reasonable. According to the 3 sigma principle, the standard deviation (SD) of parameters is set to be 0.1 (i.e. variance of 0.01). However, the results of regions excluding China (e.g. Europe and North America) under this circumstance are irrational compared to previous studies. This may be caused by the larger error in soil carbon estimate of China in BEPS. Therefore we try to reduce the SD for the other regions and test the values of 0.0707 (i.e. variance of 0.005) and 0.0316 (i.e. variance of 0.001). The results indicate that the setting of 0.1% for regions outside China and 1% for China can get a more reasonable pattern of flux. Our next work will focus on the optimal decision of constrained variance for parameters by the criterion of fit to the observation concentrations at sites. We have added these explanations in the revised paper (see lines 30-34, page 9 and lines 1-5, page 10 for details).

Specific Comments:

Comment: P14271L10 note that we don't calculate the PDF by minimizing differences, that's for
calculating the maximum likelihood estimate

Response: Thanks for this comment. We have corrected this sentence in the revised paper, as follow:
"... Enting (1995, 2002) suggested to use a prior flux to regularize the inverted flux based on the Bayesian theory, which is referred to Bayesian synthesis inversion method (BSIM). The solution of BSIM usually corresponds to the minimum of a quadratic cost function in least square sense under the assumption of Gaussian PDFs."
For details, please refer to lines 10-14, page 2.

Comment: P14276-7 I am confused about the time windows here. Is there perhaps an error? e.g. We hear that the system is run from time t-1 over l steps but the observations
listed are at t+1, t+2 ... t+l-1, should this be t-1?

Response: Thanks for this comment. This is not an error. The observation concentration c_t represents the concentration at the end of *t*th week, while the flux s_t represents the weekly average flux during the *t*th week. The c_t includes the influence from initial condition at *t*-1 and the tracer emission s_t, called the initial condition term and the source term, respectively. If we want to estimate the flux s_t, we need to run the system *l* steps forward starting from time *t*-1 (See Fig.1) to get the responses at *t*, *t*+1,..., *t*+*l*-1to the initial concentration. Then the differences between these responses and observation concentrations are caused by the emission fluxes $\{\boldsymbol{s}_t, \boldsymbol{s}_{t+1}, \dots, \boldsymbol{s}_{t-l+1}\}$ and hence can be used to estimate them.

Comment: P14281 You note that fire and fossil fluxes are not perfectly known and are excluded from the optimization. You need, then, to include their uncertainty in the observational error you use.

Response: Thanks for this suggestion. We agree with your idea that the observational error actually includes the uncertainty of fire and fossil flux emission. Neglecting their uncertainties will increase the error of optimized fluxes. Therefore, we included an extra contribution of $(0.175\text{ppm})^2$ to the observational error (See Eq.(14)). We added this explanation in the revised paper (see lines 13-16, page 10).

Comment: P14289 The comparison of posterior simulation and observations is a good idea but highlights some of the problems

Response: Thanks for this comment. Yes, the comparison of concentrations indicates some problems e.g. the inability to capture the peak and the valley and seasonal cycle identified in the residual series. We also explained in this manuscript that this may be caused by the inability of BEPS to simulate the large summer sinks (lines 25-32, page 16). Therefore we will make more efforts to improve the prior flux in terms of seasonal sink pattern in the future

work. These problems help us identify gaps in GCAS-DOM as well as BEPS and provide useful directions for further development.

References:

Deng, F., Chen, J. M., Ishizawa, M., Yuan, C. W., Mo, G., Higughi, K., Chan, D., and Maksyutov, S.: Global monthly CO_2 flux inversion with a focus over North America, Tellus B, 59, 179–190, 2007.
Deng, F. and Chen, J. M.: Recent global CO_2 flux inferred from atmospheric CO_2 observations and its regional analyses, Biogeosciences, 8, 3263–3281, doi:10.5194/bg-8-3263-2011, 2011.

Gurney, K. R., Law, R. M., Denning, A. et al.: TransCom 3 CO_2 inversion intercomparison: 1. Annual mean control results and sensitivity to transport and prior flux information, Tellus B, 55, 555–579, 2003.

Gurney, K. R., Law, R. M., Denning, A. S., et al.: Transcom 3 inversion intercomparison: model mean results for the estimation of seasonal carbon sources and sinks, Global Biogeochem. Cy., 18, GB1010, doi:10.1029/2003GB002111, 2004.

Lokupitiya, R. S., Zupanski, D., Denning, A. S., Kawa, S. R., Gurney, K. R., and Zupanski, M.: Estimation of global CO2 fluxes at regional scale using the maximum likelihood ensemble filter, J. Geophys. Res-Atmos., 113, D20110, doi:10.1029/2007JD009679, 2008.

Nassar, R., Jones, D. B. A., Kulawik, S. S., et al.: Inverse modeling of CO2 sources and sinks using satellite observations of CO2 from TES and surface flask measurements, Atmos. Chem. Phys., 11, 6029-6047, 2011.

Peters, W., Jacobson, A. R., Sweeney, C. et al.: An atmospheric perspective on North American carbon dioxide exchange: CarbonTracker, P. Natl. Acad. Sci. USA, 104, 18925–18930, 2007.
Peters, W., Krol, M. C., Van Der Werf, G. R. et al.: Seven years of recent European net terrestrial carbon dioxide exchange constrained by atmospheric observations, Glob. Change Biol., 16, 1317– 1337, 2010.

Peylin, P., Rayner, P. J., Bousquet, P., Carouge, C., Hourdin, F., Heinrich, P., Ciais, P., and AEROCARB Contributors: Daily CO_2 flux estimates over Europe from continuous atmospheric measurements: 1, inverse methodology, Atmospheric Chemistry and Physics, 5, 3173–3186, doi:10.5194/acp-5-3173-2005, http://www.atmos-chem-phys.net/5/3173/2005/, 2005.

Zheng, H., Li, Y., Chen, J. M., Wang, T., Huang, Q., and Sheng, Y.: Applying a dual optimization method to quantify carbon fluxes: recent progress in carbon flux inversion, Chinese Sci. Bull., 59, 222–226, doi:10.1007/s11434-013-0016-5, 2014

Response to Anonymous Referee #2

We would like to thank the anonymous referee 2# for the constructive comments on our manuscript Paper. Those comments are all valuable and very helpful for revising and improving our paper. Please find our response to these comments below.

Comment: H. Zheng et al. present in their manuscript 'A global carbon assimilation system based on a dual optimisation method' an inversion of 8 years of atmospheric CO2 data to estimate terrestrial and oceanic CO2 fluxes. The authors use what they call a 'dual optimisation' method to solve for scaling factors of terrestrial oceanic flux patterns based on prior fluxes obtained from the terrestrial ecosystem model BEPS and CarbonTracker output in the case of the ocean. These scaling factors are differentiated by BEPS plant functional types and latitudinal zones. In addition, the authors also solve for the fluxes directly, that represents the dual optimisation method. The manuscript is not very clear in its methodology description. Therefore it is unclear if the flux is solved for globally or per gridcell on a 1x1 degree resolution.

Response: Thank you for this comment as it indeed helps us to improve the methodology description in our paper. In fact, the flux in the application is solved for grid cells on a 1x1 degree resolution which includes 64 800 (180*360) elements at each week. For the application to 1x1 degree flux estimation, the length of the flux we solved in Eq. (12) is actually 388 800 (64800*6) at a 6-week-window, and the estimate of the earliest week in the window is left as the optimized fluxes of its corresponding time (See Sec 2.2 about the time-stepping). In response to this suggestion, two paragraphs on the dimension of fluxes and parameters aimed to estimate have been added in the revision paper (see lines 31-33, page 4, lines 1-6, page 5 and lines 17-20, page 11). The introduction of parametric model from the view of spatial coordinates followed by its vector form may be a better expression to understand the inversion in grid resolution. Then the description on the dimension of unknown states in a six-week window can help to understand the computation more clearly.

Comment: Besides this unclearity there is a major problem with the set-up of this inversion system. The authors write that they use optimised ocean fluxes from CarbonTracker as their prior ocean fluxes (p14284, ll 26/27). Since the optimised CarbonTracker ocean flux has been derived from essentially the same atmospheric CO2 observations as used in this study for the inversion, the prior ocean flux is then of course not independent form the CO2 concentration used in this study constituting a double usage of the observational data. This has to be fixed before one can analyse and draw any conclusions from the results.

Response: Thank you for this comment. We agree that the usage of optimized ocean fluxes from CarbonTracker in our system could result in a reuse of observational information. We were also conscious of this issue when doing this application, and we can still offer some explanations of this problem. Firstly, we used 312 sites from the GLOBALVIEW2010 data set

in our assimilation system while CarbonTracker only used about 100 sites (available from http://www.esrl.noaa.gov/gmd/ccgg/carbontracker/CT2010/documentation_obs.html#ct_doc). So nearly two thirds of observational data is independent from the ocean fluxes we use as an input. Secondly, we made a test on a 2.8×2.8 degree grid cell by using the ocean fluxes computed from OPA-PISCES-T model (a state-of-the-art combined global ocean circulation (OPA) and biogeochemistry model (PISCES–T, Buitenhuis et al., 2006)) and the optimized CarbonTracker ocean flux as inputs respectively with all other things being equal. The optimized ocean fluxes from these two inputs are close, so we use the CarbonTracker ocean flux as our prior ocean flux in this article to reduce the running time of the GCAS-DOM. Moreover, the oceanic fluxes before and after optimization are very similar and the optimized oceanic flux is more close to the results of CT2011_oi compared to the prior flux. It also indicates the rationality of the usage of the CarbonTracker ocean flux.

References:

Buitenhuis, E., Le Quéré, C., Aumont, O., Beaugrand, G., Bunker, A., Hirst, A., Ikeda, T., O'Brien, T., Piontkovski, S., and Straile, D.: Biogeochemical fluxes through mesozooplankton, Global Biogeochem. Cy., 20, GB2003, doi:10.1029/2005GB002511, 2006.

Manuscript prepared for Biogeosciences
with version 2014/09/16 7.15 Copernicus papers of the LaTeX class copernicus.cls.
Date: 16 January 2015

A global carbon assimilation system based on a dual optimization method

H. Zheng[1], Y. Li[1], J. M. Chen[2,3], T. Wang[4], Q. Huang[1], W. X. Huang[1], L. H. Wang[1], S. M. Li[1], W. P. Yuan[5], X. Zheng[5], S. P. Zhang[5], Z. Q. Chen[5], and F. Jiang[3]

[1]Department of Statistics, School of Mathematical Sciences, Beijing Normal University, Beijing 100875, China
[2]Department of Geography and Program in Planning, University of Toronto, Toronto M5S 3G3, Canada
[3]International Institute of Earth System Science, Nanjing University, Nanjing 210093, China
[4]Department of Mathematics and Statistics, University of Otago, Dunedin 9016, New Zealand
[5]College of Global Change and Earth System Science, Beijing Normal University, Beijing 100875, China

Correspondence to: Y. Li (liyong@bnu.edu.cn) and J. M. Chen (jing.chen@utoronto.ca)

Abstract. Ecological models are effective tools to simulate the distribution of global carbon sources and sinks. However, these models often suffer from substantial biases due to inaccurate simulations of complex ecological processes. We introduce a set of scaling factors (parameters) to an ecological model on the basis of plant functional type (PFT) and latitudes. A global carbon assimilation system (GCAS-DOM) is developed by employing a Dual Optimization Method (DOM) to invert the time-dependent ecological model parameter state and the net carbon flux state simultaneously. We use GCAS-DOM to estimate the global distribution of the CO_2 flux on $1^\circ \times 1^\circ$ grid cells for the period from ~~2000~~ 2001 to 2007. Results show that land and ocean absorb ~~-3.69 ± 0.49~~ -3.63 ± 0.50 Pg C year^{-1} and ~~-1.91 ± 0.16~~ -1.82 ± 0.16 Pg C year^{-1}, respectively. North America, Europe and China contribute ~~-0.96 ± 0.15~~ -0.98 ± 0.15 Pg C year^{-1}, -0.42 ± 0.08 Pg C year^{-1} and ~~-0.21 ± 0.28~~ -0.20 ± 0.29 Pg C year^{-1}, respectively. The uncertainties in the flux after optimization by GCAS-DOM have been remarkably reduced by more than 60 %. Through parameter optimization, GCAS-DOM can provide improved estimates of the carbon flux for each PFT. Coniferous forest (-0.97 ± 0.27 Pg C year^{-1}) is the largest contributor to the global carbon sink. Fluxes of once-dominant deciduous forest generated by BEPS is reduced to ~~-0.79 ± 0.22~~ -0.78 ± 0.23 Pg C year^{-1}, being the third largest carbon sink.

1 Introduction

The spatiotemporal distribution of carbon sources and sinks has drawn much attention in global carbon cycle research as carbon dioxide is one of the major greenhouse gases. Techniques used to quantify the spatial pattern of carbon fluxes has evolved during the past decades among which atmospheric inversion (e.g., Enting and Mansbridge, 1989; Law, 1999; Gurney et al., 2002; Röenbeck et al., 2003; Deng et al., 2007; Deng and Chen, 2011; Jiang et al., 2013; Peylin et al., 2013) is one of the most commonly used techniques.

Atmospheric inversion uses CO_2 observations to infer the distribution of the carbon flux from global (Patra et al., 2005; Rödenbeck, 2005; Rayner et al., 2008; Maki et al., 2010) to regional scales (Gerbig et al., 2003; Peylin et al., 2005; Peters et al., 2007; Schuh et al., 2010). It involves an atmospheric transport model to link the measured CO_2 concentration in the atmosphere to the surface CO_2 flux. However, the measurements from sparsely located observational sites are not sufficient for estimating global carbon sources and sinks in fine grids. Enting (1995, 2002) suggested to use a prior flux to regularize the inverted flux based on the Bayesian theory, which is referred to Bayesian synthesis inversion method (BSIM). The ~~posterior flux is determined by minimizing the difference between simulated and observed concentrations and between posterior and prior fluxes~~solution of BSIM usually corresponds to the minimum of a quadratic cost function in least square sense under the assumption of Gaussian probability distribution functions(PDFs).

In BSIM, the prior information is normally precalculated from an ecological model, e.g., Carnegie-Ames-Stanford Approach (CASA) Biosphere model (Gurney et al., 2003, 2004; Baker et al., 2006), Simple Biosphere model (SiB, Sellers et al., 1986) and Boreal Ecosystems Productivity Simulator (BEPS) model (Deng et al., 2007; Deng and Chen, 2011). These process-based models are constructed to estimate carbon sources and sinks based on the mechanisms of photosynthesis, autotrophic respiration, organic matter decomposition and nutrient cycling. However, their estimates of carbon sources and sinks at regional scales often have substantial biases, and the purpose of atmospheric inversion is to reduce these biases using the additional information of atmospheric CO_2 concentration. Atmospheric inversion methods differ considerably in the inverted carbon flux distribution among large regions of the globe (Peylin et al., 2013), and therefore improvements are still needed in the prior flux estimation and the optimization using atmospheric CO_2 data.

In consideration of the possible biases in the prior flux produced by an ecological model, ~~scaling factors are introduced to~~ Michalak et al. (2004) used "the model of the mean of the surface flux distribution" with unknown drift coefficients to substitute the prior flux ~~to correct the biases (,~~ in the BSIM. This geostatistical approach took into account the spatiotemporal correlation of the surface fluxes and hence can recover flux variations on a significantly smaller scale than typical Bayesian inversions. Different from Michalak et al. (2004), Peters et al. (2007), 2010; ~~; ;) .~~ Zupanski et al. (2007); Lokupitiya et al. (2008); Schuh et al. (2010)) introduced scaling factors to the prior flux from ecological models (e.g. SiB and CASA) to correct the biases. In these methods, a forecast

model for the scaling factors is combined with an atmospheric transport model to realize the flux evolution over time. The choice of the forecast model is usually empirical. Most researchers defined an identity operator as the forecast model for the biases (Zupanski et al., 2007; Lokupitiya et al., 2008), while Peters et al. (2007, 2010) considered a more complex forecast model which combines the information of biases in two steps before the current time step. An Ensemble Kalman Filter (Evensen, 2007) is often used for estimating the unknown scaling factors and the posterior flux is the prior flux scaled by the estimated scaling factors. This ensemble-based assimilation method takes relatively long time to warm the system to reach a stable estimation of these scaling factors, and the filtering divergence (e.g., Houtekamer and Mitchell, 1998) that retards the converge of the estimate towards observations is still a problem.

Zheng et al. (2014) proposed a dual optimization method (DOM) to estimate both the scaling factors (hereinafter known as parameters) of an ecological model and gridded carbon fluxes. DOM introduces a scaled ecological model designed by plant functional types (PFTs), and uses CO_2 observations to invert the unknown states of the parameters and net flux simultaneously. This is different from Michalak et al. (2004) which does not need to give prior estimates and hence does not rely on the information of ecological models at all. Moreover, DOM is an objective method which depends just on the information of concentration observations and the structure of the ecological model, but no forecast model is needed. The estimation precision of fluxes can be greatly improved by the dual optimization, and the statistical properties of parameters and fluxes also provide useful information about the inversion accuracy.

As DOM inverts the flux for all regions and all times simultaneously using all observations at the same time, it requires much computational resources. Therefore, it is inconceivable to use DOM to estimate the global distribution of the carbon flux at high spatial and temporal resolutions. In this study, a moving-window method similar to that of Bruhwiler et al. (2005) is developed. Different from a batch model which uses all observations to invert fluxes for all source regions at all times simultaneously, Bruhwiler et al. (2005) adopted a temporal moving window and used the CO_2 concentration observations at the current time (the end of the window) to estimate carbon fluxes in the entire window. Considering that more observations will provide more information, we propose to use the observations in the entire time window to estimate the fluxes in this window instead of using only the observations at the current time.

Due to the difference of seasonal and meteorological conditions at different latitudes, we redesign the scaling factors by dividing the globe into several latitudinal zones. Each zone shares a set of scaling factors. The number of parameters assigned to each grid equals the number of PFTs in the grid so that one parameter is associated with one PFT. This is different from Carbon Tracker (Peters et al., 2007, 2010) in which each grid is assigned to one category based on the dominant vegetation type. On the basis of the above settings, we build a global carbon assimilation system (GCAS-DOM) by combining DOM with an atmospheric transport model (MOZART-4). The forecast of the

assimilation system is embodied in updating the background concentration field. At each step, the background CO_2 concentration is updated by running MOZART-4 forward forced with the optimized flux at the last step. Finally we use the GCAS-DOM to estimate the worldwide weekly flux in $1^\circ \times 1^\circ$ grid for a relatively long period of 87 years. Results show its accuracy in flux estimation and significant effect in uncertainty reduction.

The objectives of this study are: (1) to develop a global carbon assimilation system using DOM, i.e. GCAS-DOM for the purpose of improving the estimation of the global distribution of the carbon flux, (2) to produce with GCAS-DOM a global carbon flux field on $1^\circ \times 1^\circ$ grid cells from 2000 to 2007 and analyze the flux in terms of its long-term mean, and interannual variations for the globe and selected large regions; and (3) to investigate the impacts of atmospheric CO_2 data on the estimation of the carbon flux per PFT for the evaluation of ecosystem models. This paper is organized as follows. Section 2 consists of detailed descriptions on each component of the GCAS-DOM. It begins with the introduction of state variables in Sect. 2.1. Then in Sect. 2.2, we will show the procedure of building the GCAS-DOM by using a moving-window method. Section 2.3 presents the estimation method of state variables in a window. The calculation of the uncertainties is given in Sect. 2.4. In Sect. 3, we conduct an application to estimate the global flux in $1^\circ \times 1^\circ$ grid started with a detailed introduction to models and data use in GCAS-DOM, followed by estimated quantities and their uncertainties. Finally, we summarize our results and discuss future directions of our work in Sect. 4.

2 Methodology

GCAS-DOM consists of three major components: an ecological model and an atmospheric transport model, a moving window and the optimization module. The ecological model provides the first guess of the flux before data assimilation. The atmospheric transport model links the flux to the CO_2 mixing concentration ratio. Considering the computational feasibility, we use a temporal moving window in which the flux is optimized using the optimization algorithm DOM.

2.1 State Variables

The ecosystem model is formed to simulate the variations of carbon sources and sinks based on the mechanism of carbon cycling. As improperly simulated ecological processes could result in biases in the flux, we consider a scaled ecosystem model similar to that of Lokupitiya et al. (2008). But different from Lokupitiya et al. (2008), which adjusts ecosystem respiration (ER) and gross primary productivity (GPP) using separate scaling factors, only the net ecosystem exchange (NEE) defined as the difference between ER and GPP is scaled~~because ER is strongly associated with GPP and both of them~~ . This is because both ER and GPP are much larger than the ~~ocean flux in magnitude.~~ NEP fluxes by approximately one order of magnitude, to adjust their separate influence could lead

to spurious variations. Moreover, the strong correlation between ER and GPP could result in poor performance in stability. Hence the parametric model can be represented as

$$s(x,y) = \lambda_{\mathrm{NEE}}(x,y)s_{\mathrm{NEE}}(x,y) + \lambda_{\mathrm{OCE}}(x,y)s_{\mathrm{OCE}} + s_{\mathrm{FF}}(x,y) + s_{\mathrm{FIRE}}(x,y) + \varepsilon(x,y) \tag{1}$$

where ~~s_{OCE} is the~~ x and y denote the spatial coordinates; s is the unknown flux aimed to estimate; s_{OCE} is the first-guess ocean flux computed from an ocean exchange model; ~~s_{NEE}~~ s_{NEE} is the first-guess biospheric flux estimated from a ~~terrestrial~~ ecosystem model; ~~s_{FF} and s_{FIRE}~~ s_{FF} and s_{FIRE} are fossil fuel and fire fluxes estimated from inventory-based emissions; ~~$\boldsymbol{\lambda}_{\mathrm{NEE}}$ and $\boldsymbol{\lambda}_{\mathrm{OCE}}$ are sets of~~ λ_{NEE} and λ_{OCE} are scaling factors applied to ~~land surface fluxes and ocean fluxes; the~~ the land surface flux and the ocean flux, respectively; and ε is the model error. To simplify this expression, we use its vector form:

$$\boldsymbol{s} = \boldsymbol{\lambda}_{\mathrm{NEE}} \cdot \boldsymbol{s}_{\mathrm{NEE}} + \boldsymbol{\lambda}_{\mathrm{OCE}} \cdot \boldsymbol{s}_{\mathrm{OCE}} + \boldsymbol{s}_{\mathrm{FF}} + \boldsymbol{s}_{\mathrm{FIRE}} + \boldsymbol{\varepsilon} \tag{2}$$

where all the variables are $n \times 1$ vectors and n denotes the number of the grids in globe; the "$\cdot$" (dot product) represents the element-by-element multiplication of two vectors with the same dimension unless one is a scalar; and $\boldsymbol{\varepsilon}$ is the model error with zero mean and covariance matrix $\mathbf{Q}$. Here, the ~~parameters~~ parameter vectors ($\boldsymbol{\lambda}_{\mathrm{NEE}}, \boldsymbol{\lambda}_{\mathrm{OCE}}$) and $\boldsymbol{s}$ are treated as state variables and called parameter states and flux ~~state~~states, respectively.

Zheng et al. (2014) suggests to specify the structure of parameters according to PFT to avoid over-adjustment or excessive computation. In consideration of the fact that (1) the seasonal variation in climate in the North Pole is opposite to that in the South Pole, and (2) the tropical rainforest has high temperature all year around, it is not effective to specify parameter states just according to PFT. In this study, we divide the globe into q zones according to latitude and assume that the vegetation distribution is mapped onto p PFTs. Thus a grid box can contain up to $p+1$ different types (p PFTs and 1 oceanic type) quantified with an areal fraction for each PFT in the grid.

We decompose the flux in each grid box into $p+1$ components with each denoting the flux generated from one PFT. To facilitate the expression, we use $\boldsymbol{s}^{m,j}$ for the gridded flux in the jth latitude zone computed from land and oceanic models, and it is denoted as follows

$$\boldsymbol{s}^{m,j} = \begin{pmatrix} \boldsymbol{s}^j_{\mathrm{OCE}} & \boldsymbol{s}^j_{\mathrm{NEE},1} & \boldsymbol{s}^j_{\mathrm{NEE},2} & \cdots & \boldsymbol{s}^j_{\mathrm{NEE},p} \end{pmatrix}, \qquad j = 1,2,\ldots,q \tag{3}$$

where $\boldsymbol{s}^j_{\mathrm{OCE}}$ is a vector for the oceanic component and $\boldsymbol{s}^j_{\mathrm{NEE},i}$ is a vector for the terrestrial component for the ith PFT. Gridded fluxes at the same latitude zone share the same set of parameters and thus the corresponding parameter for the $\boldsymbol{s}^{m,j}$ is

$$\boldsymbol{\lambda}^j = \begin{pmatrix} \lambda^j_{\mathrm{OCE}} & \lambda^j_{\mathrm{NEE},1} & \lambda^j_{\mathrm{NEE},2} & \cdots & \lambda^j_{\mathrm{NEE},p} \end{pmatrix}^{\mathrm{T}},$$

where each element is a ~~scaler~~ scalar used to scale the corresponding column vector of $\boldsymbol{s}^{m,j}$.

Then model (2) can be rewritten as

$$\boldsymbol{s} = \begin{pmatrix} \boldsymbol{s}^{m,1} & & & \\ & \boldsymbol{s}^{m,2} & & \\ & & \ddots & \\ & & & \boldsymbol{s}^{m,q} \end{pmatrix} \begin{pmatrix} \boldsymbol{\lambda}^1 \\ \boldsymbol{\lambda}^2 \\ \vdots \\ \boldsymbol{\lambda}^q \end{pmatrix} + \boldsymbol{s}_{\text{FF}} + \boldsymbol{s}_{\text{FIRE}} + \boldsymbol{\varepsilon} \tag{4}$$

$$\triangleq \boldsymbol{s}^m \boldsymbol{\lambda} + \boldsymbol{s}_{\text{FF}} + \boldsymbol{s}_{\text{FIRE}} + \boldsymbol{\varepsilon}.$$

where $\boldsymbol{s}^m$, referred to the prior flux, is the reshaped form of the flux computed from the ecosystem model in the order of latitude, and $\boldsymbol{\lambda} = \begin{pmatrix} \boldsymbol{\lambda}^{1\mathrm{T}} & \boldsymbol{\lambda}^{2\mathrm{T}} & \cdots & \boldsymbol{\lambda}^{q\mathrm{T}} \end{pmatrix}^{\mathrm{T}}$ is a set of scaling factors with $(p+1)q$ unknown components; $\boldsymbol{\varepsilon}$ is the model error with zero mean and covariance matrix $\mathbf{Q}$. In Model (4), as $\boldsymbol{s}_{\text{FF}}$ and $\boldsymbol{s}_{\text{Fire}}$ are imposed without optimization, their contributions to concentration can be subtracted from the observation concentrations directly. Then model (4) can be expressed in a simplified expression:

$$\boldsymbol{s} = \boldsymbol{s}^m \boldsymbol{\lambda} + \boldsymbol{\varepsilon}. \tag{5}$$

2.2 Time-stepping

In the application of GCAS-DOM, one of the major difficulties in estimating the carbon flux is the computational cost at high resolution. For the estimation of weekly fluxes on $1^o \times 1^o$ gird cells, the dimension n in Eq. (2) will be 64 800 (180×360) for each week. That is about 3 130 400 ($64\,800 \times 48$) unknowns per year, and the relevant cost of matrix operations will be at least $3\ 130\ 400^2$ which is an immense computational burden. To overcome this difficulty, we adopt a method similar to that of Bruhwiler et al. (2005). At each time t, we use the observations of CO_2 concentration and the carbon flux in the time window between t and $t+l-1$, where l is window length which could be in days, weeks, or months. This is different from Bruhwiler et al. (2005) where only the observations at time $t+l-1$ are used. We therefore have a (t,l)-window, which uses the CO_2 concentration observations $\{\boldsymbol{c}_{t+k}, 0 \le k \le l-1\}$ and the carbon flux $\{\boldsymbol{s}_{t+k}, 0 \le k \le l-1\}$ at each time point t, where the column vector $\boldsymbol{c}_{t+k}$ represents the observed CO_2 mixing ratios of a given site at $t+k$, and the column vector $\boldsymbol{s}_{t+k}$ is the global carbon flux in the time period from $t+k-1$ to $t+k$.

The time stepping in the assimilation scheme is illustrated in Fig. 1. The light shaded boxes represent the ~~the~~ prior flux at each step computed by the ecosystem model. The dark shaded boxes stand for the optimized flux. We now describe one cycle of GCAS-DOM. The first step is to use the background CO_2 concentration $C(t-1)$ as the initial value, which is a 3-D matrix for the spatial distribution of CO_2 concentration at each latitude and each longitude and each elevation. Then we run l steps of the transport model forward starting from $C(t-1)$ to get the spatial distribution of CO_2 concentration in the (t,l)-window. We keep the spatial carbon concentration patterns at all times in this window which gives $\{C(t), \ldots, C(t+l-1)\}$ and extract CO_2 mixing ratios at observation sites as $\{\boldsymbol{c}_t^b, \ldots, \boldsymbol{c}_{t+l-1}^b\}$. The second step is to estimate the optimized parameters $\{\hat{\boldsymbol{\lambda}}_{t+k}, 0 \le k \le l-1\}$

and fluxes $\{\hat{\boldsymbol{s}}_{t+k}, 0 \le k \le l-1\}$ using the resulting mixing ratios at sites $\{\boldsymbol{c}_t^b, \ldots, \boldsymbol{c}_{t+l-1}^b\}$, the observations of CO_2 concentrations in the window $\{\boldsymbol{c}_t, \ldots, \boldsymbol{c}_{t+l-1}\}$, and the prior flux in the window $\{\boldsymbol{s}_{t+k}^m, 0 \le k \le l-1\}$. The estimation method is introduced in the next section. The optimized parameter $\hat{\boldsymbol{\lambda}}_t$ and flux $\hat{\boldsymbol{s}}_t$ does not need to be estimated in the next cycle and is therefore used as ~~an estimate of the~~ estimates of the parameter and flux at time t. In the third step, we run the transport model one step forward starting from $C(t-1)$ forced with the optimized flux $\hat{\boldsymbol{s}}_t$ to get the updated spatial distribution of concentration $C'(t)$. Then we use observed CO_2 concentration to assimilate the $C'(t)$ instead of directly using it as the background concentration at time t for the next cycle in previous studies. We extract updated CO_2 concentration at locations of CO_2 observation sits from the $C'(t)$ and compare it to the observed concentration $\boldsymbol{c}_t$ at time t. A constant adjustment, which is computed from the site-averaged difference between the above two vectors, is imposed on $C'(t)$ to get an optimized spatial pattern $C(t)$ at time t.[1] In the forth step, we move the window one step forward so a new flux $\boldsymbol{s}_{t+l}^m$ and a new concentration observation $\boldsymbol{c}_{t+l}$ are read in to the system for the next computational cycle, which begins from background CO_2 concentration $C(t)$.

2.3 Adaptive DOM

In this section, we introduce the method for estimating parameters and the carbon flux in a window. Zheng et al. (2014) proposed a DOM to improve the accuracy of the optimized flux and successfully applied it to the inversion of the flux for the globe divided into 50 regions. In this study, we expect to use DOM in each (t,l)-window. As the fluxes computed for different PFTs are often correlated, direct application of the DOM to flux inversion at a high resolution will result in many abnormal estimators of parameters and large uncertainties of both parameters and fluxes. Therefore, we propose an adaptive version of DOM by adding additional regularization of scale factors which is referred to as a stochastically constrained equation (Theil and Goldberger, 1961)

$$\mathbf{1} = \boldsymbol{\lambda} + \boldsymbol{\zeta}, \tag{6}$$

where $\mathbf{1}$ is a vector with all elements equaling to 1 and $\boldsymbol{\zeta}$ is the random error of the regularization with $E(\boldsymbol{\zeta}) = 0$, and the dispersion matrix $\mathrm{var}(\boldsymbol{\zeta}) = \mathbf{W}$.

Then we will present the adaptive DOM in a (t,l)-window. To facilitate the discussion, we first introduce two denotations: (1) the observations of CO_2 concentration in (t,l)-window is denoted by a vector

$$\boldsymbol{c}^{(t,l)} = \begin{pmatrix} \boldsymbol{c}_t^{\mathrm{T}} & \boldsymbol{c}_{t+1}^{\mathrm{T}} & \cdots & \boldsymbol{c}_{t+l-1}^{\mathrm{T}} \end{pmatrix}^{\mathrm{T}}, \tag{7}$$

and named as the (t,l)-*window observation concentration*, (2) the flux is denoted as

$$\boldsymbol{s}^{(t,l)} = \begin{pmatrix} \boldsymbol{s}_t^{\mathrm{T}} & \boldsymbol{s}_{t+1}^{\mathrm{T}} & \cdots & \boldsymbol{s}_{t+l-1}^{\mathrm{T}} \end{pmatrix}^{\mathrm{T}} \tag{8}$$

[1] The correction is based on the idea that the optimized concentration should match the actually observed concentration.

and named as the (t,l)-*window flux*.

The (t,l)-window observation concentration $\boldsymbol{c}^{(t,l)}$ contains information from two sources, the (t,l)-window flux $\boldsymbol{s}^{(t,l)}$ and concentration transported from the previous time step $C(t-1)$. We let $\boldsymbol{c}^{w(t,l)}$ be the CO_2 concentration determined by $\boldsymbol{s}^{(t,l)}$, and refer it as (t,l)-window flux concentration. In fact, $\boldsymbol{c}^{w(t,l)}$ is the difference between window observation concentration $\boldsymbol{c}^{(t,l)}$ and $\{\boldsymbol{c}_t^b,\ldots,\boldsymbol{c}_{t+l-1}^b\}$ (mentioned in Sect. 2.2). Then the $\boldsymbol{c}^{w(t,l)}$ follows that

$$\boldsymbol{c}^{w(t,l)} = \mathbf{G}^{(t,l)}\boldsymbol{s}^{(t,l)} + \boldsymbol{\eta}^{(t,l)}, \tag{9}$$

where $\boldsymbol{\varepsilon}^{(t,l)}$ is the error of window concentration observation, and

$$\mathbf{G}^{(t,l)} = \begin{pmatrix} \mathbf{G}_{t,t} & & & \\ \mathbf{G}_{t+1,t} & \mathbf{G}_{t+1,t+1} & & \\ \vdots & \vdots & \ddots & \\ \mathbf{G}_{t+l-1,t} & \mathbf{G}_{t+l-1,t+1} & \cdots & \mathbf{G}_{t+l-1,t+l-1} \end{pmatrix} \tag{10}$$

is the (t,l)-window atmospheric transport matrix. It describes the contribution of the window flux to the observation sites. Each submatrix $\mathbf{G}_{m,n}$ represents the influence of the flux (normalized to 1 g C) at time n on the concentration at observation sites at time m.

In a (t,l)-window, we minimize the following objective function (11) to obtain the optimized (t,l)-window flux. This function is similar to that of DOM but with an extra penalty term, so it is called the adaptive DOM. To simplify the expression, all subscripts (t,l) are omitted here.

$$\begin{aligned} J(\boldsymbol{s},\boldsymbol{\lambda}) = &(\mathbf{G}\boldsymbol{s}-\boldsymbol{c}^w)^{\mathrm{T}}\mathbf{R}^{-1}(\mathbf{G}\boldsymbol{s}-\boldsymbol{c}^w) + (\boldsymbol{s}-\boldsymbol{s}^m\boldsymbol{\lambda})^{\mathrm{T}}\mathbf{Q}^{-1}(\boldsymbol{s}-\boldsymbol{s}^m\boldsymbol{\lambda}) \\ &+ (\boldsymbol{\lambda}-\mathbf{1})^{\mathrm{T}}\mathbf{W}^{-1}(\boldsymbol{\lambda}-\mathbf{1}) \end{aligned} \tag{11}$$

where $\boldsymbol{s}^m = \mathrm{diag}\left(\boldsymbol{s}_t^m,\ldots,\boldsymbol{s}_{t+l-1}^m\right)$ is the prior fluxes for the (t,l) window, $\mathbf{Q}$ is the error covariance matrix of the corresponding prior fluxes, $\mathbf{R}$ is the covariance matrix of the window concentration observation error $\boldsymbol{\eta}$, and $\mathbf{W}$ is the variance of constrained error.

Solving for the minimum of cost function (11) with respect to $\boldsymbol{s}$ and $\boldsymbol{\lambda}$ is similar to the process in DOM. The solutions are given by the following two equations (see Appendix A for details)

$$\begin{cases} \hat{\boldsymbol{\lambda}} = (\mathbf{X}^{\mathrm{T}}\boldsymbol{\Sigma}\mathbf{X} + \mathbf{W}^{-1})^{-1}(\mathbf{X}^{\mathrm{T}}\boldsymbol{\Sigma}\boldsymbol{c}^w + \mathbf{W}^{-1}\mathbf{1}) \\ \hat{\boldsymbol{s}} = \mathbf{Q}\mathbf{G}^{\mathrm{T}}\boldsymbol{\Sigma}(\boldsymbol{c}^w - \mathbf{G}\boldsymbol{s}^m\hat{\boldsymbol{\lambda}}) + \boldsymbol{s}^m\hat{\boldsymbol{\lambda}} \end{cases} \tag{12}$$

where $\boldsymbol{\Sigma} = (\mathbf{R}+\mathbf{G}\mathbf{Q}\mathbf{G}^{\mathrm{T}})^{-1}$, $\mathbf{X} = \mathbf{G}\boldsymbol{s}^m$ and $\hat{\boldsymbol{s}} = \begin{pmatrix} \hat{\boldsymbol{s}}_t^{\mathrm{T}} & \hat{\boldsymbol{s}}_{t+1}^{\mathrm{T}} & \cdots & \hat{\boldsymbol{s}}_{t+l-1}^{\mathrm{T}} \end{pmatrix}^{\mathrm{T}}$. As the estimation of $\hat{\boldsymbol{\lambda}}_t$ and $\hat{\boldsymbol{s}}_t$ uses the most amount of observations, it has the highest accuracy. We therefore use $\hat{\boldsymbol{\lambda}}_t$ and $\hat{\boldsymbol{s}}_t$ as the optimized parameter and carbon flux at time t.

2.4 Calculation of uncertainty

The estimators given by Eq. (12) have the following uncertainties (see Appendix A for details):

$$\begin{cases} \mathrm{var}(\hat{\boldsymbol{\lambda}}) = (\mathbf{X}^{\mathrm{T}}\boldsymbol{\Sigma}\mathbf{X} + \mathbf{W}^{-1})^{-1} \\ \mathrm{var}(\hat{\boldsymbol{s}}) = \mathbf{Q}\mathbf{G}^{\mathrm{T}}\boldsymbol{\Sigma}(\mathbf{I} - \mathbf{X}\mathrm{var}(\hat{\boldsymbol{\lambda}})\mathbf{X}^{\mathrm{T}}\boldsymbol{\Sigma})\mathbf{G}\mathbf{Q} + \boldsymbol{s}^{m}\mathrm{var}(\hat{\boldsymbol{\lambda}})(\boldsymbol{s}^{m})^{\mathrm{T}} \end{cases} \tag{13}$$

Note that the uncertainty of the parameter estimator is incorporated into the variance of estimated fluxes.

3 Application

In this section, we use the GCAS-DOM to estimate the weekly carbon flux from ~~2000~~ 2001 to 2007 on $1^\circ \times 1^\circ$ global grid cells. The assimilation system usually needs a spin-up period. Therefore the assimilation is conducted from 2000 to 2007 with the first year as a spin-up period, and the results from 2001 to 2007 are used for analysis. The initial concentration is set as a globally-uniform 3-D CO_2 field of site averaged concentration in the last week of 1999.

3.1 Ecological model

We divide the globe into $1^\circ \times 1^\circ$ grid cells, 64 800 (360×180) ~~regions~~ grids in total. GCAS-DOM uses the BEPS (Liu et al., 1997) as the terrestrial ecosystem model. BEPS simulates photosynthetic and carbon cycle processes (Chen et al., 1999; Ju et al., 2006) based on remote sensing, meteorological and soil data with a set of physical and physiological parameters related to PFT. This model is initially developed in ~~Canada and~~ North America, and then expanded for applications to the globe. The terrestrial prior fluxes is modeled by BEPS at the resolution $1^\circ \times 1^\circ$ ~~. The~~ and the weekly average values are used to avoid the problem of the diurnal cycle. The weekly oceanic flux at $1^\circ \times 1^\circ$ spatial resolution is obtained from Carbon Tracker 2010 (CT2010[2]) results (available via http://www.esrl.noaa.gov/gmd/ccgg/carbontracker/download.html).

In BEPS, vegetation is mapped onto 6 PFTs including coniferous forest, deciduous forest, evergreen forest, shrub land, C4 vegetation and "other vegetation". A grid cell can contain up to 7 different cover types (6PFTs $+1$ ocean type) with their corresponding coverage fraction. We divide equally the globe excluding China into 30 zones by latitude and each spreads a range of 6°. China is separately split into 6 zones and each spreads a range of 6° as well. Thus we yield a total of $30 + 6 = 36$ zones (see Fig. 2). In each latitude zone, there are six PFTs and 1 ocean type. As PFTs vary slowly in a short time, we assume that they are time independent within a window. Thus, we have $7 \times 36 = 252$ parameters (1 parameter corresponds to 1 PFT in a zone) to be estimated at each time step. The model error covariance matrix $\mathbf{Q}$ for the prior flux is treated using the same principle in Zhang (2013) based on the theory of statistics.

[2]CT2010 is a earlier version of Carbon Tracker released in 2011.

The constrained matrix $\mathbf{W}$ (Eq. 11) for the scaling factor is defined as a diagonal matrix with each item W_{ii} defining the degree of deviation from 1. The smaller the value is, the closer the parameter and 1 are. Conversely, the parameter can be more influenced by other information such as CO_2 measurements. We set an initial interval of [0.7, 1.3] as the range of the scaling factor $\boldsymbol{\lambda}$, as the preferences of BEPS are basically reasonable. According to the 3 sigma principle, the standard deviation (SD) of parameters is set to be 0.1 (i.e. variance of 0.01). However, the results of regions excluding China (e.g. Europe and North America) under this circumstance are irrational compared to previous studies. This may be caused by the larger error in soil carbon estimate of China in BEPS. Then we try to reduce the SD for the other regions and test the values of 0.0707 (i.e. variance of 0.005) and 0.0316 (i.e. variance of 0.001). The results indicate that the setting of 0.0316 for regions outside China and 0.1 for China can get a more reasonable pattern of flux. Therefore, we use the variance of 0.01 for the scaling factors corresponding to grids in China and 0.001 for the rest of the globe. ~~This is because we intend optimizing the flux in China by observed concentrations to a greater extent as BEPS model might generate larger error in China.~~

3.2 Background fluxes

In the process of making inference about flux from ecosystems, we need to exclude the contribution of other CO_2 fluxes such as fire and fossil fuel emissions to observed concentrations. They are not perfectly known and but also not the target of this study. Their information is included in the observation data we use. As mentioned in Sect. 2.1, we do not include any parameters concerning fossil fuel and fire fluxes in the optimization. So the contribution of fossil fuel and fire emissions need to be extracted from the window flux concentration. Then the window flux concentration excluding the influence of fire and fossil fuel is used in the process of ecosystem flux optimization. Although the fire and fossil fluxes are excluded from our optimization, their uncertainties should be considered into the observational error. Therefore, we included an extra contribution of $(0.175\ \text{ppm})^2$ to the observational error (See Eq.14).

The fossil fuel and fire fluxes are from the CT2010 results on $1^\circ \times 1^\circ$ resolution. The annual summary of fossil fuel and fire emissions is listed in Table 1.

3.3 Atmospheric transport model

The carbon fluxes of the earth's surface at a certain time affect the CO_2 concentration observed in a subsequent time period in the atmosphere. Therefore, we can use the atmospheric CO_2 concentration to invert the historical distribution of carbon fluxes. Atmospheric transport models are generally used to describe the process of surface fluxes spreading into the atmosphere. The commonly employed transport models include MUGCM (Law, 1993), NCAR (Erickson et al., 1996), TM5 (Krol et al., 2005), and MOZART-4 (Emmons et al., 2010). We will use MOZART-4 in our study as its implementation is flexible. MOZART-4 divides the space from the earth surface to a height of

2 hPa into 28 vertical sigma-pressure layers, and its horizontal resolution can be adjusted according to the capacity of computers. The highest resolution by far has been $0.7^\circ \times 0.7^\circ$. We use the meteorological data from the National Centers for Environmental Prediction (NCEP) reanalysis data (http://www.esrl.noaa.gov/psd/data/gridded/data.ncep.reanalysis.html).

This model here is used in two forms. In its full form, the assimilation is done by running forward with the optimized flux state at the previous time step to update the historical space concentration at the current time. In its simplified form, the model is slightly reduced by leaving out the influence of window flux on the site concentrations, and is shown as a transport matrix (see Eq. 10).

3.4 Concentration data

Weekly average observations of CO_2 concentration are from GLOBALVIEW-2011 dataset (http://www.esrl.noaa.gov/gmd/ccgg/obspack/data.php). These data consist of pseudo-weekly interpolation CO_2 concentration data measured at 312 global sites. The map of stations is shown in Fig. 3. As the residual standard deviations (RSD) of the CO_2 concentration data given by the var files in GLOBALVIEW-2011 dataset are in months, we convert them onto weekly value by linear interpolation, and impose a floor of 0.175 ppm to the data uncertainty using the equation (Deng et al., 2007)

$$\mathbf{R} = \sqrt{(0.175\,\mathrm{ppm})^2 + \mathrm{RSD}^2}, \tag{14}$$

where 0.175 ppm is the system error at each site.

3.5 Window length

The choice of the window length is an important issue in assimilation systems. The longer a window size is, the more overlapping of transport integrations and the larger calculation demand are. However, a small window size will cause significant errors. Peters et al. (2005, 2007, 2010) used a five-week smoothing window. Here, we choose a six-week smoothing window, which is sufficiently long for the fluxes to transmit across the world.

As scale factors vary much more slowly than the fluxes themselves ((Zupanski et al., 2007)), it is reasonable that the scale factor is time-independent within a six-week window but varies among different windows. Therefore, the unknown states aimed to estimate involve 252 parameters and 388 800 (64 800 grids$\times$6 weeks) fluxes for each six-week step.

3.6 Results

In this section, we will firstly show the variations of estimated scaling factors over time. Then the total optimized flux and its uncertainties will be summarized to compare with those of the prior flux and results from previous studies. We focus on the result of three large regions of North America, Europe and China. Moreover, we further study the quantities and seasonal variations of fluxes for 6

PFTs. The spatial distribution of the optimized flux is shown in a map of $1^\circ \times 1^\circ$ grid cell. We also show the fit of the optimized concentrations to the observation concentrations to evaluate the system.

3.6.1 Optimized parameters

Figure 4 shows the results of the scaling factors for 6 PFTs and an oceanic type in the latitude zone spread from 24° N to 30° N excluding China. The estimators fluctuate around 1 with small volatility. If the value is larger than 1, it means that the absolute value of the prior flux is underestimated and therefore need to be multiplied by a factor more than 1 to increase its value. On the contrary, an estimator smaller than 1 indicates a decrease of the absolute value of the flux. From the time series of weekly estimates, most of the parameters show annual periodicity and the scaling factors of coniferous type indicate opposite "swings" in contrast to other PFTs. The scaling factors of deciduous and evergreen types have less amplitudes than those of the remaining types.

3.6.2 Optimized fluxes and their uncertainties

Global Carbon Budget

We compare the optimized total flux (excluding fire and fossil fuel emissions, same as thereafter) with the prior flux and the results of CT2011_oi which is a newer version of CarbonTracker released on 28 June 2013 (Fig. 5). The terrestrial fluxes make a major contribution for the year ~~2000~~ 2001 to 2007 before or after optimization. Before optimization, the annual average terrestrial and oceanic fluxes are ~~−3.16~~ −3.10 and $-1.62\,\mathrm{Pg\,C\,year^{-1}}$, respectively. GCAS-DOM increases the uptake in land and ocean by a mean value ~~0.52~~0.53 $\mathrm{Pg\,C\,year^{-1}}$ and ~~0.23~~0.20 $\mathrm{Pg\,C\,year^{-1}}$, respectively, over the ~~2000–2007~~2001–2007. Therefore the total annual ecosystem sinks show a significant increase mainly due to the increase in the terrestrial sink during the ~~8~~7 years. As the oceanic prior flux is derived from the optimized results of CT2010, the oceanic fluxes before and after optimization are very similar. Even so, the optimized oceanic flux is still more close to the results of CT2011_oi compared to the prior flux.

The optimized result indicates that the terrestrial ecosystems and oceans respectively absorb an average of ~~3.69 and 1.85~~3.63 and 1.82 $\mathrm{Pg\,C\,year^{-1}}$ over the ~~2000–2007~~ 2001–2007 period. These values compare well with the inversion results of Deng and Chen (2011), which are on average 3.63 and 1.84 $\mathrm{Pg\,C\,year^{-1}}$, respectively, for the years 2002–2007. We then further compare the net land sink and oceanic sink in our study to that of the Global Carbon Project (GCP, Table 2). The Global Carbon Budget 2013 v2.3 (Le Quéré et al., 2014) is the newest version released on April 2014 by the GCP. The net land sink of GCP is calculated by the difference of land sink and land-use change emissions in Global Carbon Budget 2013 v2.3, while that of the GCAS-DOM is computed by the difference between the terrestrial sink (Fig. 5) and fire emission in Table 1. The GCP generates larger oceanic sinks than GCAS-DOM, with the smallest gap of ~~0.1~~0.25 $\mathrm{Pg\,C\,year^{-1}}$ in ~~2000~~ 2001 and

largest difference of 0.92 $\mathrm{Pg\,C\,year^{-1}}$ in 2002. For the net land sink, the largest difference occurs in 2002 when the GCP releases 0.52 $\mathrm{Pg\,C\,year^{-1}}$ from land while the GCAS-DOM maintains a land uptake of 1.06 $\mathrm{Pg\,C\,year^{-1}}$. The ~~7~~6 year mean of the net land sink excluding the year 2002 in our study is ~~1.48~~1.38 $\mathrm{Pg\,C\,year^{-1}}$ which is close to ~~1.39~~1.29 $\mathrm{Pg\,C\,year^{-1}}$ in GCP. Figure 5 shows that the total sink in land and ocean varies considerably among years, and the variation is mostly due to the sink in land. GCAS-DOM sink results are usually larger than the prior value, indicating the prior flux underestimates the land sink. The multi-year mean values of GCAS-DOM and CT2011_oi are about the same, but they differ to some extent in individual years, suggesting that different data assimilation methods can result in considerable difference in the optimized carbon flux.

From the point of inter-annual variabilities, the ocean flux shows much smaller variability than land flux, revealing that the ocean sink pattern is stable. The inter-annual variation of the land sink suggests notable correlation with the climate change. The optimized annual flux by GCAS-DOM detects an anomaly in 2005 which shows the smallest sink. This could be mainly attributed to a continuing drought from July to September in the Amazon that affects plant growth and high temperature in 2005 which intensifies the ecosystem respiratory activities (Deng and Chen, 2011). The relatively weak sinks in 2002 and 2007 may be related to the EI Niño Southern Oscillation event in 2002–2003 and 2006–2007, respectively, that causes anomalies in precipitation causing draughts in some regions.

Before optimization, we use an uncertainty of 1.98 $\mathrm{Pg\,C\,year^{-1}}$ for the land flux, and an uncertainty of 0.93 $\mathrm{Pg\,C\,year^{-1}}$ for the oceanic flux, resulting in a total uncertainty of 2.18 $\mathrm{Pg\,C\,year^{-1}}$ for the globe. Table 3 shows the uncertainty of optimized fluxes by GCAS-DOM. We can see different levels of uncertainty reductions for land and ocean. The uncertainty of the globe is significantly reduced by about 75–80 % and ocean has the slightly larger reduction than the global value. It is mostly due to the stronger constraint by the elongated clustered observation sites over the Pacific Ocean (see Fig. 3). The uncertainty reductions of ocean and land respectively stabilize at around 82 % and 75 % for the years ~~2000–2007~~2001–2007.

4 ~~Regional Carbon Budget~~

Regional Carbon Budget

We further analyze three large regions: Europe, North America and China. As shown in Table 4, GCAS-DOM respectively increases the sink by 0.14 $\mathrm{Pg\,C\,year^{-1}}$ for Europe and ~~0.32~~0.31 $\mathrm{Pg\,C\,year^{-1}}$ for North America compared to the prior flux for the ~~eight-year~~ seven-year mean. The uncertainties before optimization (0.44 $\mathrm{Pg\,C\,year^{-1}}$ and 0.86 $\mathrm{Pg\,C\,year^{-1}}$ for Europe and North America, respectively) are reduced to 0.08 $\mathrm{Pg\,C\,year^{-1}}$ and 0.15 $\mathrm{Pg\,C\,year^{-1}}$, respectively. The uncertainty reductions for these two regions, are remarkably large at about 80 %, possibly because the atmospheric CO_2 is densely observed in these two regions. In Europe, the carbon sink from our

study ($-0.42 \pm 0.08\,\mathrm{Pg\,C\,year^{-1}}$) is higher than CT2011_oi ($-0.33 \pm 1.86\,\mathrm{Pg\,C\,year^{-1}}$), Deng and Chen (2011, $-0.22\,\mathrm{Pg\,C\,year^{-1}}$) and Jiang et al. (2013, $-0.28 \pm 0.17\,\mathrm{Pg\,C\,year^{-1}}$). In North America, our result (~~-0.96 ± 0.15~~ $-0.98 \pm 0.15\,\mathrm{Pg\,C\,year^{-1}}$) agrees well with Deng and Chen (2011, $-0.89 \pm 0.18\,\mathrm{Pg\,C\,year^{-1}}$), but shows slightly stronger sink than Jiang et al. (2013, $-0.81 \pm 0.21\,\mathrm{Pg\,C\,year^{-1}}$). In China, the carbon uptake slightly increases from the prior to ~~-0.21~~$0.20\,\mathrm{Pg\,C\,year^{-1}}$, which is weaker than Jiang et al. (2013, $-0.28 \pm 0.18\,\mathrm{Pg\,C\,year^{-1}}$) and Piao et al. (2009, $-0.35 \pm 0.33\,\mathrm{Pg\,C\,year^{-1}}$). Although the change of sink in China before and after optimization is small, the uncertainty reduction is about 67 %, which is smaller than those of Europe and North America because of relatively few atmospheric data observed within and around China.

The inter-annual variations of fluxes before and after optimization are shown in Fig. 6. With a minor fluctuation, the carbon uptake of Europe has an increasing trend before 2004, and then decreases after 2005. Similar temporal trends are also found in North America. In the first ~~five~~ four years, the carbon sink in China is stable around $-0.22\,\mathrm{Pg\,C\,year^{-1}}$, and slightly decreases from 2005 to 2007. The uncertainties of optimized fluxes for three regions vary slightly from year to year and are remarkably reduced from those of the prior fluxes.

Fluxes for each PFT

Our gridded inversion system at 1° resolution affords us the possibility to analyze the impacts of atmospheric CO_2 data on the estimation of the carbon sink by PFT. Figure 7 shows the annual mean terrestrial flux for 6 PFTs. "Prior" stands for fluxes simulated by BEPS consisting of 6 PFT components with corresponding coverage fraction in each grid, while "GCAS-DOM" represents fluxes optimized by GCAS-DOM and the statistics are based on the principle that each $1^\circ \times 1^\circ$ gridbox is assigned to a single category according to the locally dominant PFT. As shown in Fig. 7, the order of the sink magnitudes of different PFTs is altered after optimization. The carbon flux of once-dominant deciduous forests is reduced from ~~-0.96~~ 0.93 to ~~-0.79~~$0.78\,\mathrm{Pg\,C\,year^{-1}}$. After optimization, largest net uptake is shown in regions dominated by coniferous forest ($-0.97 \pm 0.27\,\mathrm{Pg\,C\,year^{-1}}$) and is increased by ~~115.68~~118.20 %. As the coniferous forest is mainly distributed in North America, Europe and part of Russia, this results in the notable increase of the sinks in North American and Europe (Table 4). This large increase in the sink magnitude for conifer from the prior estimate suggests that the ecosystem model considerably underestimates the sink for this PFT. "Other vegetation" ($-0.86 \pm 0.20\,\mathrm{Pg\,C\,year^{-1}}$) and deciduous forest (~~-0.79 ± 0.22~~ $-0.78 \pm 0.23\,\mathrm{Pg\,C\,year^{-1}}$) are respectively the second and third PFTs in terms of their total sink magnitude. Evergreen forests most located in the Southern Hemisphere absorb ~~-0.77 ± 0.21~~ $-0.72 \pm 0.22\,\mathrm{Pg\,C\,year^{-1}}$ on average. Relatively speaking, shrub land (~~-0.17 ± 0.12~~ $-0.16 \pm 0.12\,\mathrm{Pg\,C\,year^{-1}}$) and C4 vegetation (~~$-0.26 \pm 0.13$~~ $-0.25 \pm 0.13\,\mathrm{Pg\,C\,year^{-1}}$) make the least contributions to the total global carbon sink. The slight changes in the sink magnitudes of Shrub land and C4 vegetation before and after optimization suggest that BEPS provides nearly unbiased sink estimates for these two PFTs. The

sink magnitude of the "other vegetation" is modified greatly by optimization, suggesting BEPS does not work well for all other land cover types lumped into this PFT. One way to improve BEPS would be to introduce more PFTs. Through this analysis, we show that GCAS-DOM has provided a useful model framework to evaluate an ecosystem model by PFT, and it can potentially provide directions for further development of ecosystem models.

To further investigate the seasonal variation of the carbon flux, we compare the optimized weekly fluxes to the prior fluxes by PFT. For this purpose, we select the results of coniferous forest and "other vegetation" (Figs. 8 and 9), as fluxes by these two types present largest change after optimization among all PFTs. All the time series exhibit pronounced seasonality, and Northern Hemisphere and Southern Hemisphere show opposite seasonal patterns. In Northern Hemisphere, the optimized flux of coniferous forest shows a general shift towards larger sinks in all seasons from that of the prior flux. After optimization, greater net uptake is found in the growing season and smaller net source in autumn and winter. In Southern Hemisphere, the optimized flux shows a smaller seasonal amplitude than the prior flux with departures from the prior occurring in winter and summer. Note that the sink magnitude is much smaller than that of Northern Hemisphere, and therefore the optimization of the conifer flux in Southern Hemisphere does not make much difference in the overall sink estimate. For "other vegetation", similar deviations of the optimized flux from the prior flux in June through September are observed, but fluxes in other months show good agreements. In Southern Hemisphere, the optimized flux present larger amplitudes than the prior flux, and this is opposite to the case of coniferous forest.

Spatial distribution of fluxes

Figures 10 and 11 show the long-term mean spatial pattern of the flux on $1^\circ \times 1^\circ$ net before and after optimization. This flux does not include the carbon emission due to fires, and the net land sink is those shown in Figs. 10 and 11 minus fire emission. The uptakes over boreal Asia, Europe and southeastern Canada have been greatly increased by GCAS-DOM, while the sink in tropical America is slightly reduced after optimization. For the oceanic flux, a slight decrease of the source is found in Tropical Ocean. The results of this study show that relatively large sinks are located in the Northern Hemisphere continents, and tropical continental areas. The northern continental areas from 30° N to 90° N contribute the largest sink of $-2.052.07\,\mathrm{Pg\,C\,year^{-1}}$. Next, the continental areas in the range of 30° S–30° N contribute a sink of $-1.761.68\,\mathrm{Pg\,C\,year^{-1}}$. Intense sinks mainly appear in eastern US, Europe, tropical America, tropical Asia and central Africa. South continental areas (30–90° S) show an approximately neutral flux. For ocean, carbon uptake is distributed relatively evenly between north (30–90° N) and south (30–90° S), while the region 30° S–30° N generates a weak source of $0.320.33\,\mathrm{Pg\,C\,year^{-1}}$.

3.0.3 Fit to CO_2 concentrations

The fit of the simulated CO_2 concentration by GCAS-DOM to the observed concentration is an important aspect for overall evaluation of optimization. To evaluate the performance of GCAS-DOM, we run MOZART-4 forward forced by the prior flux and optimized flux, respectively, and compare the simulated time series of CO_2 concentrations to the observed concentrations. We integrate the concentration data of all the 312 sites for ~~8~~7 years to a series with ~~119 808~~104 832 (312×48 weeks ~~$\times 8$~~$\times 7$ years) elements and draw the simulated vs. observed scatterplot (Fig. 12). The blue points show an upward departure from the one-to-one line, indicating the simulated concentrations with the prior flux are overestimated. The RMSE between the simulated and observed concentrations of the 119 808 weekly data points items is significantly reduced from ~~5.49~~5.58 ppm to ~~2.74~~2.76 ppm after optimization. The correlation between the simulated and the observed concentration is also improved after optimization with R^2 increasing from ~~0.67 to 0.83~~0.64 to 0.80. This suggests that the optimized flux is a significant improvement over the prior flux.

Generally speaking, the simulated concentration at sites at Northern Hemisphere shows better agreement with the observed concentration than the sites at Southern Hemisphere. We present the seasonal cycles fitted to the simulated and observed concentration time series of two sites in Fig. 13. At Dahlen, the simulated concentrations based on the optimized flux follows closely the observed values. However, the simulated concentration based on the prior flux show an upward drift from the observed concentrations especially in the last several years. This indicates that the prior flux is biased and the cumulative effect of this bias will get progressively larger over time. This result is consistent with the viewpoint that the prior sink value is underestimated. Moreover, the green points present a seasonal cycle with smaller amplitudes. This may be due to the shortcoming in the terrestrial biosphere model which may not well describe the seasonal cycle of ecosystem processes.

At Mace Head, the simulated concentrations with the optimized flux deviate less from the observations in winter than in summer. This inability of the optimization procedure to capture the depth of summer carbon drawdown by photosynthesis was also found in CarbonTracker North America and Europe (Peters et al., 2007, 2010) and a carbon cycle assimilation system based on the Biosphere Energy Transfer Hydrology model (CCDAS, Rayner et al., 2005). One common problem would be that biospheric models tend to underestimate the carbon sink in summer and this bias is not fully rectified in the optimization process because of insufficient atmospheric CO_2 data and the significant model-data mismatch errors in the CO_2 observation. Nevertheless, the optimized concentration is still a large improvement over the case of the prior flux. In addition, it should be noted that some discontinued high anomalies in the simulated concentration with the prior flux have been remarkably ameliorated after optimization.

We also investigate the overall quality of 312 sites used in our system by week. In Fig. 14, week-by-week residuals (simulated minus observed) are made to assess the bias of the optimized CO_2 field against the observations. The errors averaged by 312 sites can be controlled within about

$\pm$0.50.51 ppm, indicating a satisfactory performance of our assimilation system. However, an obvious seasonal cycle is identified in the residual series. This is mainly caused by the generally worse fit to observed concentration at the sites in Southern Hemisphere. Although the residual error is small, the clear seasonal pattern of the residual error indicates that there is still some useful information in the CO_2 data that are not fully utilized. The inability of BEPS to simulate the large summer sinks may be part of the reason because the bias in summer is not fully corrected through optimization (as shown in Fig. 13). Our study therefore suggests that efforts should be made to improve the prior flux estimation not only in terms of the annual sink magnitude but also the seasonal sink pattern.

4 Conclusions

In this study, we build a global carbon assimilation system (GCAS-DOM) and employ GCAS-DOM to optimize a record of the globally gridded CO_2 flux at $1^\circ \times 1^\circ$ resolution for the years from 2000 2001 to 2007. This newly developed system combines the ecological model BEPS, atmospheric transport model MOZART-4 and observations of CO_2 concentration to optimize the optimize the carbon fluxparameter and carbon flux simultaneously. In consideration of errors in climate data and the structure of BEPS, we design a set of inflation parameters for optimization according to latitude and plant function type in BEPS, resulting in 252 parameters at each time step. The $1^\circ \times 1^\circ$ for flux estimation at the global scale in our study is higher than those in previous studies . This high resolution has the advantage of reducing aggregation error in each gridand therefore it would significantly advance our understanding of regional carbon cycles. To reduce the computational demand, a moving-window method is used in the system so as to obtain time-varying parameters and fluxes.

Our optimized results show that the mean terrestrial and oceanic carbon fluxes over the period of 2000–2007 are $-3.69 \pm 0.49$2001–2007 are $-3.63 \pm 0.50\,\mathrm{Pg\,C\,year^{-1}}$ and $-1.91 \pm 0.16-1.82 \pm 0.16\,\mathrm{Pg\,C\,year^{-1}}$, respectively. North America, Europe and China contribute $-0.96 \pm 0.15-0.98 \pm 0.15\,\mathrm{Pg\,C\,year^{-1}}$, $-0.42 \pm 0.08\,\mathrm{Pg\,C\,year^{-1}}$ and $-0.21 \pm 0.28-0.20 \pm 0.29\,\mathrm{Pg\,C\,year^{-1}}$, respectively. Large sinks are mainly located in the Northern Hemisphere and tropical continental areas. Moreover, the uncertainties of carbon fluxes are notably reduced by more than 60 % after optimization for the globe and aforementioned 3 regions.

Coniferous forest, deciduous forest, shrub, crop, evergreen forest, shrub land, grass, C4 plants, and other vegetation contribute to the global carbon flux at $-0.97 \pm 0.27\,\mathrm{Pg\,C\,year^{-1}}$, $-0.79 \pm 0.22-0.78 \pm 0.23\,\mathrm{Pg\,C\,year^{-1}}$, $-0.77 \pm 0.21-0.72 \pm 0.22\,\mathrm{Pg\,C\,year^{-1}}$, $-0.17 \pm 0.12-0.16 \pm 0.12\,\mathrm{Pg\,C\,year^{-1}}$, $-0.26 \pm 0.13-0.25 \pm 0.13\,\mathrm{Pg\,C\,year^{-1}}$, $-0.86 \pm 0.20\,\mathrm{Pg\,C\,year^{-1}}$, respectively. The optimized flux of conifer differs most from its prior, indicating that the biospheric model BEPS might have the largest error for this PFT. Shrub land and C4 vegetation show only slight changes from the prior after optimization. In terms of seasonal variation, the optimized flux shows larger uptake in growing season than the priors for coniferous

forest and "other vegetation" in Northern Hemisphere. In Southern Hemisphere, the optimized flux of coniferous forest shows a reduced amplitude from its prior, while the opposite occurs for "other vegetation".

After the flux optimization by GCAS-DOM, the agreement between the simulated and observed CO_2 concentrations is greatly improved (R^2 increased from ~~0.67 to 0.83~~0.64 to 0.80, and RMSE reduced from ~~5.49 to 2.74~~5.58 to 2.76 ppm). However the residual differences between simulated and observed concentrations show some seasonal structure, indicating that some deficiency in the prior flux that has not been rectified in the optimization process. Since atmospheric CO_2 data are sparse, errors in the biospheric model used to produce the prior flux can propagate to the final optimization results. Further effort is needed to improve photosynthesis and respiration calculation in BEPS in order to reduce the biases in the flux estimation in both summer and winter.

Appendix A: Proof of Eqs. (11) and (12)

According to the theory of DOM, for any fixed $\boldsymbol{\lambda}$, the optimized $\boldsymbol{s}$ that achieves the minimum of cost function (11) is

$$\boldsymbol{s}(\boldsymbol{\lambda}) = \mathbf{Q}\mathbf{G}^{\mathrm{T}}\boldsymbol{\Sigma}^{-1}(\boldsymbol{c}^{w} - \mathbf{G}\boldsymbol{s}^{m}\boldsymbol{\lambda}) + \boldsymbol{s}^{m}\boldsymbol{\lambda}, \tag{A1}$$

where $\boldsymbol{\Sigma} = (\mathbf{R} + \mathbf{G}\mathbf{Q}\mathbf{G}^{\mathrm{T}})$.

Plug Eq. (A1) into the cost function (11), we can get

$$\begin{aligned} J(\boldsymbol{\lambda}) &= (\mathbf{G}\boldsymbol{s}(\boldsymbol{\lambda}) - \boldsymbol{c}^{w})^{\mathrm{T}}\mathbf{R}^{-1}(\mathbf{G}\boldsymbol{s}(\boldsymbol{\lambda}) - \boldsymbol{c}^{w}) + (\boldsymbol{s}(\boldsymbol{\lambda}) - \boldsymbol{s}^{m}\boldsymbol{\lambda})^{\mathrm{T}}\mathbf{Q}^{-1}(\boldsymbol{s}(\boldsymbol{\lambda}) - \boldsymbol{s}^{m}\boldsymbol{\lambda}) \\ &\quad + (\boldsymbol{\lambda} - \mathbf{1})^{\mathrm{T}}\mathbf{W}^{-1}(\boldsymbol{\lambda} - \mathbf{1}) \\ &= (\mathbf{X}\boldsymbol{\lambda} - \boldsymbol{c}^{w})^{\mathrm{T}}\boldsymbol{\Sigma}^{-1}(\mathbf{X}\boldsymbol{\lambda} - \boldsymbol{c}^{w}) + (\boldsymbol{\lambda} - \mathbf{1})^{\mathrm{T}}\mathbf{W}^{-1}(\boldsymbol{\lambda} - \mathbf{1}) \end{aligned} \tag{A2}$$

where $\mathbf{X} = \mathbf{G}\boldsymbol{s}^{m}$ and the first item is referred to the DOM. Then the optimized estimator $\hat{\boldsymbol{\lambda}}$ is easy to get by derivation of Eq. (A2) with respective to $\boldsymbol{\lambda}$

$$\hat{\boldsymbol{\lambda}} = (\mathbf{X}^{\mathrm{T}}\boldsymbol{\Sigma}^{-1}\mathbf{X} + \mathbf{W}^{-1})^{-1}(\mathbf{X}^{\mathrm{T}}\boldsymbol{\Sigma}^{-1}\boldsymbol{c}^{w} + \mathbf{W}^{-1}\mathbf{1}) \tag{A3}$$

Thus the optimized fluxes can be obtained by replacing $\boldsymbol{\lambda}$ in the (A1) by the $\hat{\boldsymbol{\lambda}}$.

Note that

$$\boldsymbol{c}^{w} = \mathbf{G}\boldsymbol{s} + \boldsymbol{\eta} = \mathbf{G}(\boldsymbol{s}^{m}\boldsymbol{\lambda} + \boldsymbol{\varepsilon}) + \boldsymbol{\eta} = \mathbf{X}\boldsymbol{\lambda} + \boldsymbol{\gamma}, \tag{A4}$$

where $E(\boldsymbol{\gamma}) = 0, \mathrm{var}(\boldsymbol{\gamma}) = \boldsymbol{\Sigma}$ and $\mathbf{1}$ can be treated as a random error with expectation $\boldsymbol{\lambda}$ and variance matrix $\mathbf{W}$. It is not hard to obtain the variance of $\hat{\boldsymbol{\lambda}}$.

$$\mathrm{var}(\hat{\boldsymbol{\lambda}}) = (\mathbf{X}^{\mathrm{T}}\boldsymbol{\Sigma}\mathbf{X} + \mathbf{W}^{-1})^{-1}. \tag{A5}$$

The variance of $\hat{\boldsymbol{s}}$

$$\mathrm{var}(\hat{\boldsymbol{s}}) = \mathrm{var}(\mathbf{Q}\mathbf{G}^{\mathrm{T}}\boldsymbol{\Sigma}^{-1}(\boldsymbol{c}^{w} - \mathbf{G}\boldsymbol{s}^{m}\hat{\boldsymbol{\lambda}}) + \boldsymbol{s}^{m}\hat{\boldsymbol{\lambda}})$$

$$
\begin{aligned}
&= \mathrm{var}(\mathbf{Q}\mathbf{G}^{\mathrm{T}}\boldsymbol{\Sigma}^{-1}(\boldsymbol{c}^{w} - \mathbf{G}\boldsymbol{s}^{m}(\mathbf{X}^{\mathrm{T}}\boldsymbol{\Sigma}^{-1}\mathbf{X} + \mathbf{W}^{-1})^{-1}(\mathbf{X}^{\mathrm{T}}\boldsymbol{\Sigma}^{-1}\boldsymbol{c}^{w} + \mathbf{W}^{-1}\mathbf{1})) \\
&\quad + \boldsymbol{s}^{m}(\mathbf{X}^{\mathrm{T}}\boldsymbol{\Sigma}^{-1}\mathbf{X} + \mathbf{W}^{-1})^{-1}(\mathbf{X}^{\mathrm{T}}\boldsymbol{\Sigma}^{-1}\boldsymbol{c}^{w} + \mathbf{W}^{-1}\mathbf{1})) \\
&= \mathrm{var}((\mathbf{Q}\mathbf{G}^{\mathrm{T}}\boldsymbol{\Sigma}^{-1} - \mathbf{Q}\mathbf{G}^{\mathrm{T}}\boldsymbol{\Sigma}^{-1}\mathbf{X}\mathrm{var}(\hat{\boldsymbol{\lambda}})\mathbf{X}^{\mathrm{T}}\boldsymbol{\Sigma}^{-1} + \boldsymbol{s}^{m}\mathrm{var}(\hat{\boldsymbol{\lambda}})\mathbf{X}^{\mathrm{T}}\boldsymbol{\Sigma}^{-1})\boldsymbol{c}^{w}) \\
&\quad + \mathrm{var}((\boldsymbol{s}^{m}\mathrm{var}(\hat{\boldsymbol{\lambda}})\mathbf{W}^{-1} - \mathbf{Q}\mathbf{G}^{\mathrm{T}}\boldsymbol{\Sigma}^{-1}\mathbf{X}\mathrm{var}(\hat{\boldsymbol{\lambda}})\mathbf{W}^{-1})\mathbf{1})
\end{aligned} \tag{A6}
$$

where

$$
\begin{aligned}
&\mathrm{var}((\boldsymbol{s}^{m}\mathrm{var}(\hat{\boldsymbol{\lambda}})\mathbf{W}^{-1} - \mathbf{Q}\mathbf{G}^{\mathrm{T}}\boldsymbol{\Sigma}^{-1}\mathbf{X}\mathrm{var}(\hat{\boldsymbol{\lambda}})\mathbf{W}^{-1})\mathbf{1}) \\
&\quad = (\boldsymbol{s}^{m}\mathrm{var}(\hat{\boldsymbol{\lambda}}) - \mathbf{Q}\mathbf{G}^{\mathrm{T}}\boldsymbol{\Sigma}^{-1}\mathbf{X}\mathrm{var}(\hat{\boldsymbol{\lambda}}))(\mathbf{W}^{-1}\mathrm{var}(\hat{\boldsymbol{\lambda}})(\boldsymbol{s}^{m})^{\mathrm{T}} - \mathbf{W}^{-1}\mathrm{var}(\hat{\boldsymbol{\lambda}})\mathbf{X}^{\mathrm{T}}\boldsymbol{\Sigma}^{-1}\mathbf{G}\mathbf{Q}) \\
&\quad = \mathbf{Q}\mathbf{G}^{\mathrm{T}}\boldsymbol{\Sigma}^{-1}\mathbf{X}\mathrm{var}(\hat{\boldsymbol{\lambda}})\mathbf{W}^{-1}\mathrm{var}(\hat{\boldsymbol{\lambda}})\mathbf{X}^{\mathrm{T}}\boldsymbol{\Sigma}^{-1}\mathbf{G}\mathbf{Q} - \mathrm{var}(\hat{\boldsymbol{\lambda}})\mathbf{W}^{-1}\mathrm{var}(\hat{\boldsymbol{\lambda}})\mathbf{X}^{\mathrm{T}}\boldsymbol{\Sigma}^{-1}\mathbf{G}\mathbf{Q} - \\
&\mathbf{Q}\mathbf{G}^{\mathrm{T}}\boldsymbol{\Sigma}^{-1}\mathbf{X}\mathrm{var}(\hat{\boldsymbol{\lambda}})\mathbf{W}^{-1}\mathrm{var}(\hat{\boldsymbol{\lambda}})(\boldsymbol{s}^{m})^{\mathrm{T}} + \boldsymbol{s}^{m}\mathrm{var}(\hat{\boldsymbol{\lambda}})\mathbf{W}^{-1}\mathrm{var}(\hat{\boldsymbol{\lambda}})(\boldsymbol{s}^{m})^{\mathrm{T}}
\end{aligned} \tag{A7}
$$

and

$$
\begin{aligned}
&\mathrm{var}((\mathbf{Q}\mathbf{G}^{\mathrm{T}}\boldsymbol{\Sigma}^{-1} - \mathbf{Q}\mathbf{G}^{\mathrm{T}}\boldsymbol{\Sigma}^{-1}\mathbf{X}\mathrm{var}(\hat{\boldsymbol{\lambda}})\mathbf{X}^{\mathrm{T}}\boldsymbol{\Sigma}^{-1} + \boldsymbol{s}^{m}\mathrm{var}(\hat{\boldsymbol{\lambda}})\mathbf{X}^{\mathrm{T}}\boldsymbol{\Sigma}^{-1})\boldsymbol{c}^{w}) \\
&\quad = (\mathbf{Q}\mathbf{G}^{\mathrm{T}}\boldsymbol{\Sigma}^{-1} - \mathbf{Q}\mathbf{G}^{\mathrm{T}}\boldsymbol{\Sigma}^{-1}\mathbf{X}\mathrm{var}(\hat{\boldsymbol{\lambda}})\mathbf{X}^{\mathrm{T}}\boldsymbol{\Sigma}^{-1} + \boldsymbol{s}^{m}\mathrm{var}(\hat{\boldsymbol{\lambda}})\mathbf{X}^{\mathrm{T}}\boldsymbol{\Sigma}^{-1})\boldsymbol{\Sigma} \\
&(\boldsymbol{\Sigma}^{-1}\mathbf{G}\mathbf{Q} - \boldsymbol{\Sigma}^{-1}\mathbf{X}\mathrm{var}(\hat{\boldsymbol{\lambda}})\mathbf{X}^{\mathrm{T}}\boldsymbol{\Sigma}^{-1}\mathbf{G}\mathbf{Q} + \boldsymbol{\Sigma}^{-1}\mathbf{X}\mathrm{var}(\hat{\boldsymbol{\lambda}})(\boldsymbol{s}^{m})^{\mathrm{T}}) \\
&\quad = (\mathbf{Q}\mathbf{G}^{\mathrm{T}} - \mathbf{Q}\mathbf{G}^{\mathrm{T}}\boldsymbol{\Sigma}^{-1}\mathbf{X}\mathrm{var}(\hat{\boldsymbol{\lambda}})\mathbf{X}^{\mathrm{T}} + \boldsymbol{s}^{m}\mathrm{var}(\hat{\boldsymbol{\lambda}})\mathbf{X}^{\mathrm{T}}) \\
&(\boldsymbol{\Sigma}^{-1}\mathbf{G}\mathbf{Q} - \boldsymbol{\Sigma}^{-1}\mathbf{X}\mathrm{var}(\hat{\boldsymbol{\lambda}})\mathbf{X}^{\mathrm{T}}\boldsymbol{\Sigma}^{-1}\mathbf{G}\mathbf{Q} + \boldsymbol{\Sigma}^{-1}\mathbf{X}\mathrm{var}(\hat{\boldsymbol{\lambda}})(\boldsymbol{s}^{m})^{\mathrm{T}}) \\
&\quad = \mathbf{Q}\mathbf{G}^{\mathrm{T}}\boldsymbol{\Sigma}^{-1}\mathbf{G}\mathbf{Q} - \mathbf{Q}\mathbf{G}^{\mathrm{T}}\boldsymbol{\Sigma}^{-1}XA^{-1}\mathbf{X}^{\mathrm{T}}\boldsymbol{\Sigma}^{-1}\mathbf{G}\mathbf{Q} + \mathbf{Q}\mathbf{G}^{\mathrm{T}}\boldsymbol{\Sigma}^{-1}\mathbf{X}\mathrm{var}(\hat{\boldsymbol{\lambda}})(\boldsymbol{s}^{m})^{\mathrm{T}} - \\
&\mathbf{Q}\mathbf{G}^{\mathrm{T}}\boldsymbol{\Sigma}^{-1}\mathbf{X}\mathrm{var}(\hat{\boldsymbol{\lambda}})\mathbf{X}^{\mathrm{T}}\boldsymbol{\Sigma}^{-1}\mathbf{G}\mathbf{Q} + \mathbf{Q}\mathbf{G}^{\mathrm{T}}\boldsymbol{\Sigma}^{-1}\mathbf{X}\mathrm{var}(\hat{\boldsymbol{\lambda}})\mathbf{X}^{\mathrm{T}}\boldsymbol{\Sigma}^{-1}\mathbf{X}\mathrm{var}(\hat{\boldsymbol{\lambda}})\mathbf{X}^{\mathrm{T}}\boldsymbol{\Sigma}^{-1}\mathbf{G}\mathbf{Q} \\
&- \mathbf{Q}\mathbf{G}^{\mathrm{T}}\boldsymbol{\Sigma}^{-1}\mathbf{X}\mathrm{var}(\hat{\boldsymbol{\lambda}})\mathbf{X}^{\mathrm{T}}\boldsymbol{\Sigma}^{-1}\mathbf{X}\mathrm{var}(\hat{\boldsymbol{\lambda}})(\boldsymbol{s}^{m})^{\mathrm{T}} + \boldsymbol{s}^{m}\mathrm{var}(\hat{\boldsymbol{\lambda}})\mathbf{X}^{\mathrm{T}}\boldsymbol{\Sigma}^{-1}\mathbf{G}\mathbf{Q} - \\
&\boldsymbol{s}^{m}\mathrm{var}(\hat{\boldsymbol{\lambda}})\mathbf{X}^{\mathrm{T}}\boldsymbol{\Sigma}^{-1}\mathbf{X}\mathrm{var}(\hat{\boldsymbol{\lambda}})\mathbf{X}^{\mathrm{T}}\boldsymbol{\Sigma}^{-1}\mathbf{G}\mathbf{Q} + \boldsymbol{s}^{m}\mathrm{var}(\hat{\boldsymbol{\lambda}})\mathbf{X}^{\mathrm{T}}\boldsymbol{\Sigma}^{-1}\mathbf{X}\mathrm{var}(\hat{\boldsymbol{\lambda}})(\boldsymbol{s}^{m})^{\mathrm{T}}
\end{aligned} \tag{A8}
$$

Combining Eqs. (A7) and (A8), we can get

$$
\begin{aligned}
\mathrm{var}(\hat{\boldsymbol{s}}) &= \boldsymbol{s}^{m}\mathrm{var}(\hat{\boldsymbol{\lambda}})(\boldsymbol{s}^{m})^{\mathrm{T}} + \mathbf{Q}\mathbf{G}^{\mathrm{T}}\boldsymbol{\Sigma}^{-1}\mathbf{G}\mathbf{Q} - \mathbf{Q}\mathbf{G}^{\mathrm{T}}\boldsymbol{\Sigma}^{-1}\mathbf{X}\mathrm{var}(\hat{\boldsymbol{\lambda}})\mathbf{X}^{\mathrm{T}}\boldsymbol{\Sigma}^{-1}\mathbf{G}\mathbf{Q} \\
&= \mathbf{Q}\mathbf{G}^{\mathrm{T}}\boldsymbol{\Sigma}^{-1}(\mathbf{I} - \mathbf{X}\mathrm{var}(\hat{\boldsymbol{\lambda}})\mathbf{X}^{\mathrm{T}}\boldsymbol{\Sigma}^{-1})\mathbf{G}\mathbf{Q} + \boldsymbol{s}^{m}\mathrm{var}(\hat{\boldsymbol{\lambda}})(\boldsymbol{s}^{m})^{\mathrm{T}}
\end{aligned} \tag{A9}
$$

Acknowledgements. This work was supported by the National Key Basic Research Development Program of China (Grant No. 2010CB950703)

References

Baker, D. F., Law, R. M., Gurney, K. R., Rayner, P., Peylin, P., Denning, A. S., Bousquet, P., Bruhwiler, L., Chen, Y.-H., Ciais, P., Fung, I. Y., Heimann, M., John, J., Maki, T., Maksyutov, S., Masarie, K., Prather, M., Pak, B., Taguchi, S., and Zhu, Z.: TransCom 3 inversion intercomparison: Impact of transport model errors on the interannual variability of regional CO_2 fluxes, 1988–2003, Global Biogeochem. Cy., 20, GB1002, doi:10.1029/2004GB002439, 2006.

Bruhwiler, L. M. P., Michalak, A. M., Peters, W., Baker, D. F., and Tans, P.: An improved Kalman Smoother for atmospheric inversions, Atmos. Chem. Phys., 5, 2691–2702, doi:10.5194/acp-5-2691-2005, 2005.

Chen, J. M., Liu, J., Cihlar, J., and Goulden, M. L.: Daily canopy photosynthesis model through temporal and spatial scaling for remote sensing applications, Ecol. Model., 124, 99–119, 1999.

Deng, F. and Chen, J. M.: Recent global CO_2 flux inferred from atmospheric CO_2 observations and its regional analyses, Biogeosciences, 8, 3263–3281, doi:10.5194/bg-8-3263-2011, 2011.

Deng, F., Chen, J. M., Ishizawa, M., Yuan, C. W., Mo, G., Higughi, K., Chan, D., and Maksyutov, S.: Global monthly CO_2 flux inversion with a focus over North America, Tellus B, 59, 179–190, 2007.

Emmons, L. K., Walters, S., Hess, P. G., Lamarque, J.-F., Pfister, G. G., Fillmore, D., Granier, C., Guenther, A., Kinnison, D., Laepple, T., Orlando, J., Tie, X., Tyndall, G., Wiedinmyer, C., Baughcum, S. L., and Kloster, S.: Description and evaluation of the Model for Ozone and Related chemical Tracers, version 4 (MOZART-4), Geosci. Model Dev., 3, 43–67, doi:10.5194/gmd-3-43-2010, 2010.

Enting, I. G.: Inverse Problems in Atmospheric Constituent Transport, Cambridge Atmospheric and Space Science Series, Cambridge University Press, 2002.

Enting, I. G. and Mansbridge, J. V.: Seasonal sources and sinks of atmospheric CO_2: direct inversion of filtered data, Tellus B, 41, 111–126, 1989.

Enting, I. G., Trudinger, C. M., and Francey, R. J: a synthesis inversion of the concentration and $\delta^{13}C$ of atmospheric CO_2, Tellus B, 47, 35–52, 1995.

Erickson, D. J., Rasch, P. J., Tans, P. P., Friedlingstein, P., Ciais, P., Maier-Reimer, E., Six, K., Fischer, C. A., and Walters, S.: The seasonal cycle of atmospheric CO_2: a study based on the NCAR Community Climate Model (CCM2), J. Geophys. Res.-Atmos., 101, 15079–15097, 1996.

Evensen, G.: Data Assimilation: the Ensemble Kalman Filter, Springer, Berlin, 2007.

Gerbig, C., Lin, J. C., Wofsy, S. C., Daube, B. C., Andrews, A. E., Stephens, B. B., Bakwin, P. S., and Grainger, C. A.: Toward constraining regional-scale fluxes of CO_2 with atmospheric observations over a continent: 1. Observed spatial variability from airborne platforms, J. Geophys. Res., 108, 4756, doi:10.1029/2002JD003018, 2003.

Gurney, K. R., Law, R. M., Denning, A., Rayner, P. J., Baker, D., Bousquet, P., Bruhwiler, L., Chen, Y. H., Ciais, P., Fan, S., Fung, I. Y., Gloor, M., Heimann, M., Higuchi, K., John, J., Maki, T., Maksyutov, S., Masarie, K., Peylin, P., Prather, M., Pak, B. C., Randerson, J., Sarmiento, J., Taguchi, S., Takahashi, T., and Yuen, C. W.: Towards robust regional estimates of CO_2 sources and sinks using atmospheric transport models, Nature, 415, 626–630, 2002.

Gurney, K. R., Law, R. M., Denning, A., Rayner, P. J., Baker, D., Bousquet, P., Bruhwiler, L., Chen, Y. H., Ciais, P., Fan, S., Fung, I. Y., Gloor, M., Heimann, M., Higuchi, K., John, J., Kowalczyk, E., Maki, T., Maksyutov, S., Peylin, P., Prather, M., Pak, B. C., Sarmiento, J., Taguchi, S., Takahashi, T., and Yuen, C. W.:

TransCom 3 CO_2 inversion intercomparison: 1. Annual mean control results and sensitivity to transport and prior flux information, Tellus B, 55, 555–579, 2003.

Gurney, K. R., Law, R. M., Denning, A. S., Rayner, P., Pak, B. C., Baker, D., Bousquet, P., Bruhwiler, L., Chen, Y. H., Ciais, P., Fung, I. Y., Heimann, M., John, J., Maki, T., Maksyutov, S., Peylin, P., Prather, M., and Taguchi, S.: Transcom 3 inversion intercomparison: model mean results for the estimation of seasonal carbon sources and sinks, Global Biogeochem. Cy., 18, GB1010, doi:10.1029/2003GB002111, 2004.

Houtekamer, P. L. and Mitchell, H. L.: Data assimilation using an ensemble Kalman filter technique, Mon. Weather Rev., 126, 796–811, 1998.

Jiang, F., Wang, H. W., Chen, J. M., Zhou, L. X., Ju, W. M., Ding, A. J., Liu, L. X., and Peters, W.: Nested atmospheric inversion for the terrestrial carbon sources and sinks in China, Biogeosciences, 10, 5311–5324, doi:10.5194/bg-10-5311-2013, 2013.

Ju, W. M., Chen, J. M., Black, T. A., Barr, A. G., Liu, J., and Chen, B. Z.: Modelling multi-year coupled carbon and water fluxes in a boreal aspen forest, Agr. Forest Meteorol., 140, 136–151, 2006.

~~Kaminski, T., Rayner, P. J., Heimann, M., and Enting, I. G.: On aggregation errors in atmospheric transport inversions, J. Geophys. Res., 106, 4703–4715, 2001.~~

Krol, M., Houweling, S., Bregman, B., van den Broek, M., Segers, A., van Velthoven, P., Peters, W., Dentener, F., and Bergamaschi, P.: The two-way nested global chemistry-transport zoom model TM5: algorithm and applications, Atmos. Chem. Phys., 5, 417–432, doi:10.5194/acp-5-417-2005, 2005.

Law, R. M.: Modelling the Global Transport of Atmospheric Constituents, Ph.D. thesis, School of Earth Sciences, University of Melbourne, Parkvile, Victoria, Australia, 1993.

Law, R. M.: CO_2 sources from a mass-balance inversion: sensitivity to the surface constraint, Tellus B, 51, 254–265, 1999.

Le Quéré, C., Peters, G. P., Andres, R. J., Andrew, R. M., Boden, T. A., Ciais, P., Friedlingstein, P., Houghton, R. A., Marland, G., Moriarty, R., Sitch, S., Tans, P., Arneth, A., Arvanitis, A., Bakker, D. C. E., Bopp, L., Canadell, J. G., Chini, L. P., Doney, S. C., Harper, A., Harris, I., House, J. I., Jain, A. K., Jones, S. D., Kato, E., Keeling, R. F., Klein Goldewijk, K., Körtzinger, A., Koven, C., Lefèvre, N., Maignan, F., Omar, A., Ono, T., Park, G.-H., Pfeil, B., Poulter, B., Raupach, M. R., Regnier, P., Rödenbeck, C., Saito, S., Schwinger, J., Segschneider, J., Stocker, B. D., Takahashi, T., Tilbrook, B., van Heuven, S., Viovy, N., Wanninkhof, R., Wiltshire, A., and Zaehle, S.: Global carbon budget 2013, Earth Syst. Sci. Data, 6, 235–263, doi:10.5194/essd-6-235-2014, 2014.

Liu, J., Chen, J. M., Cihlar, J., and Park, W. M.: A process-based boreal ecosystem productivity simulator using remote sensing inputs, Remote Sens. Environ., 62, 158–175, 1997.

Lokupitiya, R. S., Zupanski, D., Denning, A. S., Kawa, S. R., Gurney, K. R., and Zupanski, M.: Estimation of global CO_2 fluxes at regional scale using the maximum likelihood ensemble filter, J. Geophys. Res-Atmos., 113, D20110, doi:10.1029/2007JD009679, 2008.

Michalak, A. M., Bruhwiler, L., and Tans, P. P.: A geostatistical approach to surface flux estimation of atmospheric trace gases, J. Geophys. Res., 109, D14109, doi:10.1029/2003JD004422, 2004.

Maki, T., Ikegami, M., Fujita, T., Hirahara, T., Yamada, K., Mori, K., Takeuchi, A., Tsutsumi, Y., Suda, K., and Conway, T. J.: New technique to analyse global distributions of CO_2 concentrations and fluxes from non-processed observational data, Tellus B, 62, 797–809, 2010.

Patra, P. K., Maksyutov, S., Ishizawa, M., Nakazawa, T., Takahashi, T., and Ukita, J.: Interannual and decadal changes in the sea–air CO_2 flux from atmospheric CO_2 inverse modeling, Global Biogeochem. Cy., 19, GB4013, doi:10.1029/2004GB002257, 2005.

Peters, W., Miller, J. B., Whitaker, J., Denning, A. S., Hirsch, A., Krol, M. C., Zupanski, D., Bruhwiler, L., and Tans, P. P.: An ensemble data assimilation system to estimate CO_2 surface fluxes from atmospheric trace gas observations., J. Geophys. Res., 110, D24304, doi:10.1029/2005JD006157, 2005.

Peters, W., Jacobson, A. R., Sweeney, C., Andrews, A. E., Conway, T. J., Masarie, K., Miller, J. B., Bruhwiler, L. M. P., Pétron, G., Hirsch, A. I., Worthy, D. E. J., van der Werf, G. R., Randerson, J. T., Wennberg, P. O., Krol, M. C., and Tans, P. P.: An atmospheric perspective on North American carbon dioxide exchange: CarbonTracker, P. Natl. Acad. Sci. USA, 104, 18925–18930, 2007.

Peters, W., Krol, M. C., Van Der Werf, G. R., Houweling, S., Jones, C. D., Hughes, J., Schaefer, K., Masarie, K. A., Jacobson, A. R., Miller, J. B., Cho, C. H., Ramonet, M., Schmidt, M., Ciattaglia, L., Apadula, F., Heltal, D., Meinhardt, F., Di Sarra, A. G., Piacentino, S., Sferlazzo, D., Aalto, T., Hatakka, J., Ström, J., Haszpra, L., Meijer, H., Van Der Laan, S., Neubert, R. E. M., Jordan, A., Rodó, X., Morgui, J.-A., Vermulen, A. T., Popa, E., Rozanski, K., Zimnoch, M., Manning, A. C., Leuenberger, M., Uglietti, C., Dolman, A. J., Ciais, P., Heimann, M., and Tans, P. P.: Seven years of recent European net terrestrial carbon dioxide exchange constrained by atmospheric observations, Glob. Change Biol., 16, 1317–1337, 2010.

Peylin, P., Rayner, P. J., Bousquet, P., Carouge, C., Hourdin, F., Heinrich, P., Ciais, P., and AEROCARB contributors: Daily CO_2 flux estimates over Europe from continuous atmospheric measurements: 1, inverse methodology, Atmos. Chem. Phys., 5, 3173–3186, doi:10.5194/acp-5-3173-2005, 2005.

Peylin, P., Law, R. M., Gurney, K. R., Chevallier, F., Jacobson, A. R., Maki, T., Niwa, Y., Patra, P. K., Peters, W., Rayner, P. J., Rödenbeck, C., van der Laan-Luijkx, I. T., and Zhang, X.: Global atmospheric carbon budget: results from an ensemble of atmospheric CO_2 inversions, Biogeosciences, 10, 6699–6720, doi:10.5194/bg-10-6699-2013, 2013.

Piao, S., Fang, J., Ciais, P., Peylin, P., Huang, Y., Sitch, S., and Wang, T.: The carbon balance of terrestrial ecosystems in China, Nature, 458, 1009–1013, 2009.

Rayner, P. J., Scholze, M., Knorr, W., Kaminski, T., Giering, R., and Widmann, H.: Two decades of terrestrial carbon fluxes from a carbon cycle data assimilation system (CCDAS), Global Biogeochem. Cy., 19, GB2026, doi:10.1029/2004GB002254, 2005.

Rayner, P. J., Law, R. M., Allison, C. E., Francey, R. J., Trudinger, C. M., and Pickett-Heaps, C.: Interannual variability of the global carbon cycle (1992–2005) inferred by inversion of atmospheric CO_2 and $d^{13}CO_2$ measurements, Global Biogeochem. Cy., 22, GB3008, doi:10.1029/2007GB003068, 2008.

Rödenbeck, C.: Estimating CO_2 Sources and Sinks from Atmospheric Mixing Ratio Measurements Using a Global Inversion of Atmospheric Transport, Technical report 6, Max Planck Institute for Biogeochemistry, Jena, 2005.

Röenbeck, C., Houweling, S., Gloor, M., and Heimann, M.: Timedependent atmospheric CO_2 inversions based on interannually varying tracer transport, Tellus B, 55, 488–497, 2003.

Sellers, P. J., Mintz, Y., Sud, Y. C., and Dalcher, A.: A Simple Biosphere Model (SIB) for Use within General Circulation Models, J. Atmos. Sci., 43, 505–531, 1986.

Schuh, A. E., Denning, A. S., Corbin, K. D., Baker, I. T., Uliasz, M., Parazoo, N., Andrews, A. E., and Worthy, D. E. J.: A regional high-resolution carbon flux inversion of North America for 2004, Biogeosciences, 7, 1625–1644, doi:10.5194/bg-7-1625-2010, 2010.

Theil, H. and Goldberger, A. S.: On pure and mixed statistical estimation in economics, Int. Econ. Rev., 2, 65–78, 1961.

Zhang, Y. J.: The non-parametric estmation of error matrix in the carbon flux, Master's thesis, School of Mathematical Sciences, Beijing Normal University, 2013 (in Chinese).

Zheng, H., Li, Y., Chen, J. M., Wang, T., Huang, Q., and Sheng, Y.: Applying a dual optimization method to quantify carbon fluxes: recent progress in carbon flux inversion, Chinese Sci. Bull., 59, 222–226, doi:10.1007/s11434-013-0016-5, ~~2013.~~ 2014.

Zupanski, D., Denning, A. S., Uliasz, M., Zupanski, M., Schuh, A. E., Rayner, P., Peters, W., and Corbin, K. D.: Carbon flux bias estimation employing maximum likelihood ensemble filter (MLEF), J. Geophys. Res-Atmos., 112, D17107, doi:10.1029/2006JD008371, 2007.

Table 1. Annual fossil fuel and fire emissions across ~~2000–2007~~ 2001–2007 (in $\mathrm{Pg\,C\,year^{-1}}$).

Year	Fossil Fuel	Fire
~~2000 7.0196 2.0574~~ 2001	7.1527	2.1868
2002	7.2069	2.4057
2003	7.5434	2.2687
2004	7.9537	2.3422
2005	8.1887	2.3541
2006	8.4376	2.1479
2007	8.6908	2.3267

Table 2. Comparison of the optimized carbon sinks in this study with the "Global Carbon Budget 2013 v2.3" (in $\mathrm{Pg\,C\,year^{-1}}$).

	GCP		GCAS-DOM	
Year	Net land sink	Oceanic sink	Net land sink	Oceanic sink
~~2000 −1.99 −2.14 −2.08 −2.04~~ 2001	−1.14	−1.95	−1.77	−1.70
2002	(0.52)*	−2.45	−1.06	−1.53
2003	−0.24	−2.42	−1.59	−1.68
2004	−2.06	−2.33	−1.52	−1.87
2005	−0.53	−2.43	−0.77	−1.78
2006	−2.17	−2.51	−1.50	−2.19
2007	−1.57	−2.55	−1.14	−2.00

* "(0.52)" represents the carbon resource of 0.52 $\mathrm{Pg\,C\,year^{-1}}$.

Table 3. The uncertainties of optimized fluxes for the globe, land and ocean by GCAS-DOM (in $\mathrm{Pg\,C\,year^{-1}}$).

Year	~~2000~~2001	2002	2003	2004	2005	2006	2007
Globe	~~0.47~~ 0.51	0.50	0.53	0.52	0.54	0.54	0.53
Land	~~0.44~~ 0.48	0.47	0.51	0.50	0.51	0.51	0.50
Ocean	0.16	~~0.16~~ 0.17	0.15	0.16	0.17	0.16	0.15

Table 4. Comparison of the long-term mean optimized carbon fluxes by GCAS-DOM with previous studies during ~~2000–2007~~2001–2007.

Region	Europe	North America	China
Model	-0.28 ± 0.44	~~-0.64 ± 0.86~~ -0.67 ± 0.86	-0.17 ± 0.87
GCAS-DOM	-0.42 ± 0.08	~~-0.96 ± 0.15~~ -0.98 ± 0.15	~~-0.21 ± 0.28~~ -0.20 ± 0.29
CT2011_oi	~~-0.33 ± 1.86~~ -0.32 ± 1.84	~~-0.66 ± 1.39~~ -0.66 ± 1.35	-0.26
Deng and Chen (2011)[a]	-0.22	-0.89 ± 0.18	–
Jiang et al. (2013)[b]	-0.28 ± 0.17	-0.81 ± 0.21	-0.28 ± 0.18
Piao et al. (2009)[c]	–	–	-0.35 ± 0.33

[a] Mean from 2002 to 2007.

[b] Mean from 2002 to 2008.

[c] Mean from 1996 to 2005, and the result is based on inversion method.

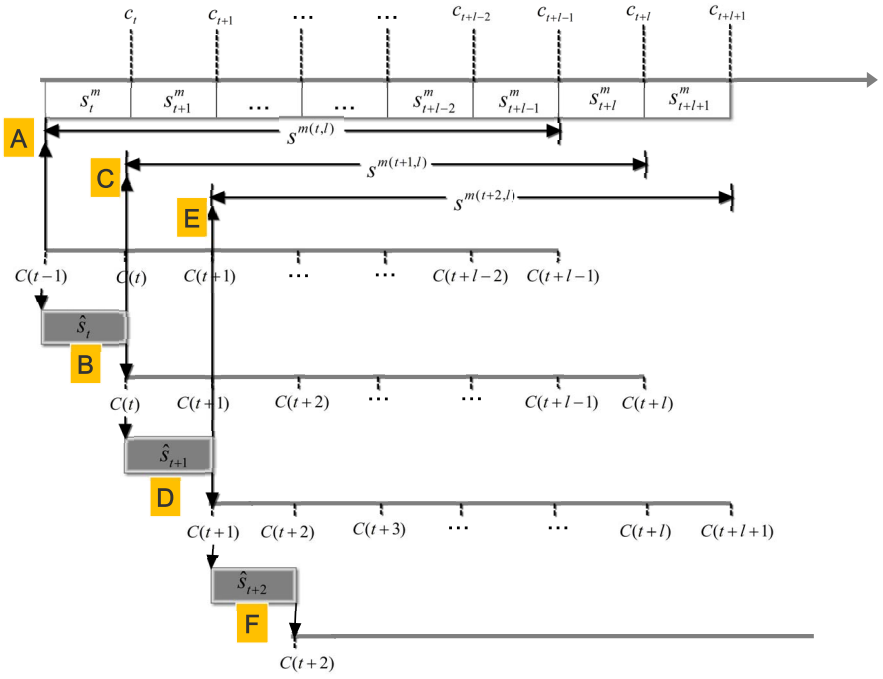

Figure 1. Illustration of three cycles in GCAS-DOM in which a state vector composes of the flux at l steps.

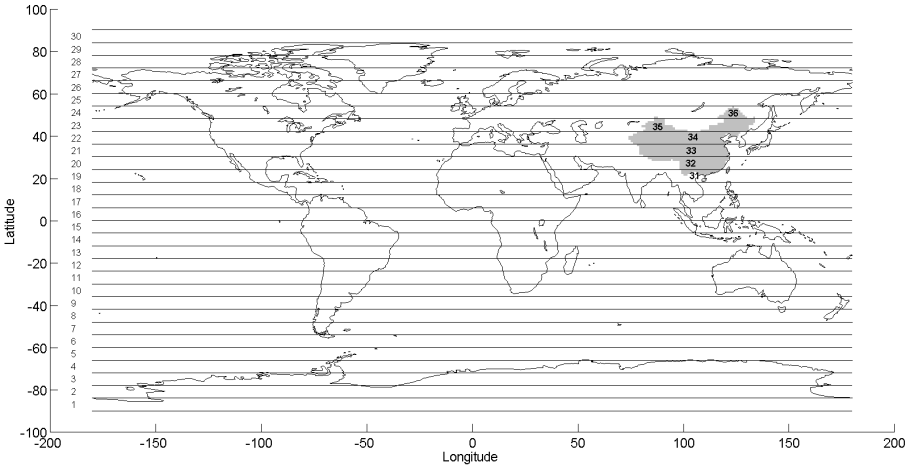

Figure 2. The partition of zones in globe.

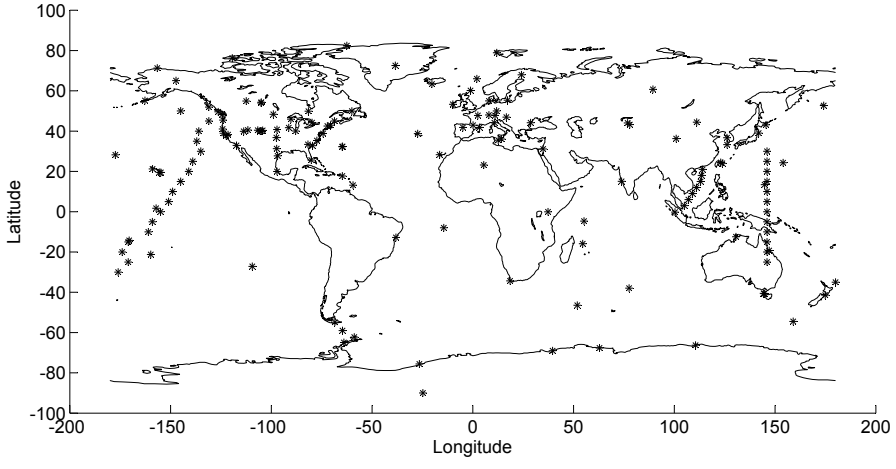

Figure 3. The distribution of 312 stations used in this study. The x-axis and y-axis stand for longitude and latitude respectively. The sign " * " represents the location of sites.

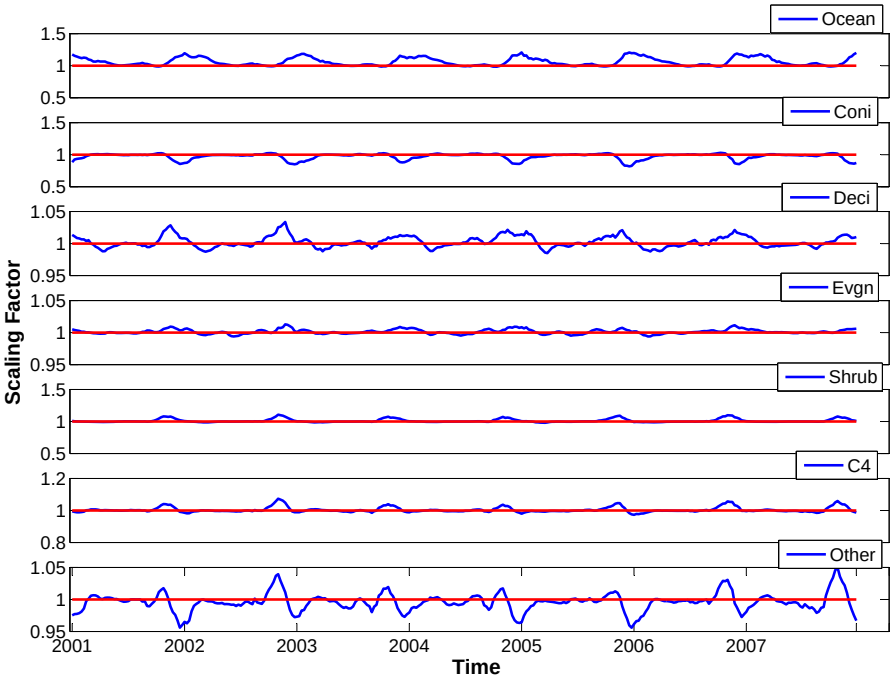

Figure 4. The results of optimized weekly scaling factors in the 20th latitude zone, where Coni stands for coniferous forest, Deci for deciduous forest, Evgn for evergreen forest, Shrub for shrub land, C4 for C4 vegetation and Other for other vegetation. Blue lines are estimated parameters, while Red lines are constants which equal to 1. Note different scales are used.

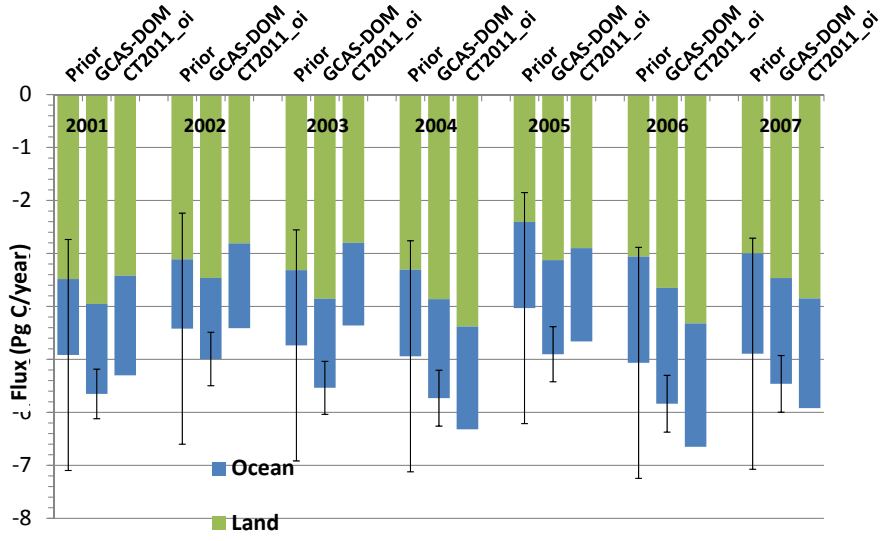

Figure 5. Annual fluxes for the land and ocean from ~~2000~~ 2001 to 2007 in comparison with results of CT2011_oi. "Prior", "GCAS-DOM" are the fluxes before and after optimization. Black horizontal lines denote the uncertainties of global flux. The uncertainties of global flux from CT2011_oi are averagely about 6 $\mathrm{Pg\,C\,year^{-1}}$ which is not shown in this figure. All units are in $\mathrm{Pg\,C\,year^{-1}}$. The fossil fuel and fire emissions are excluded here.

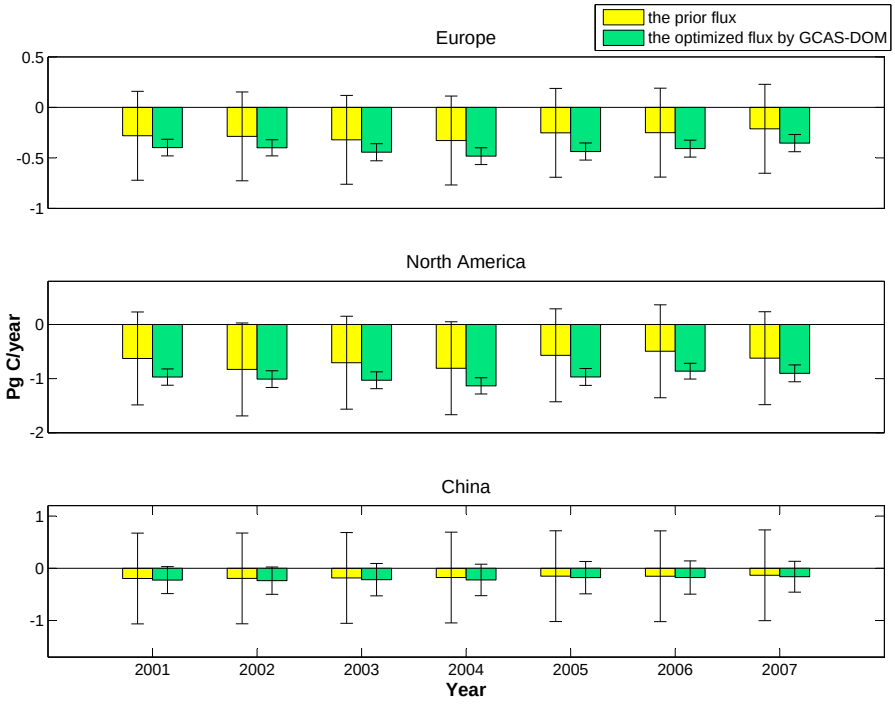

Figure 6. Fluxes and their uncertainties in three large regions before and after optimization from ~~2000~~ 2001 to 2007 (in $\mathrm{Pg\,C\,year^{-1}}$) **(a)** Europe **(b)** North America **(c)** China.

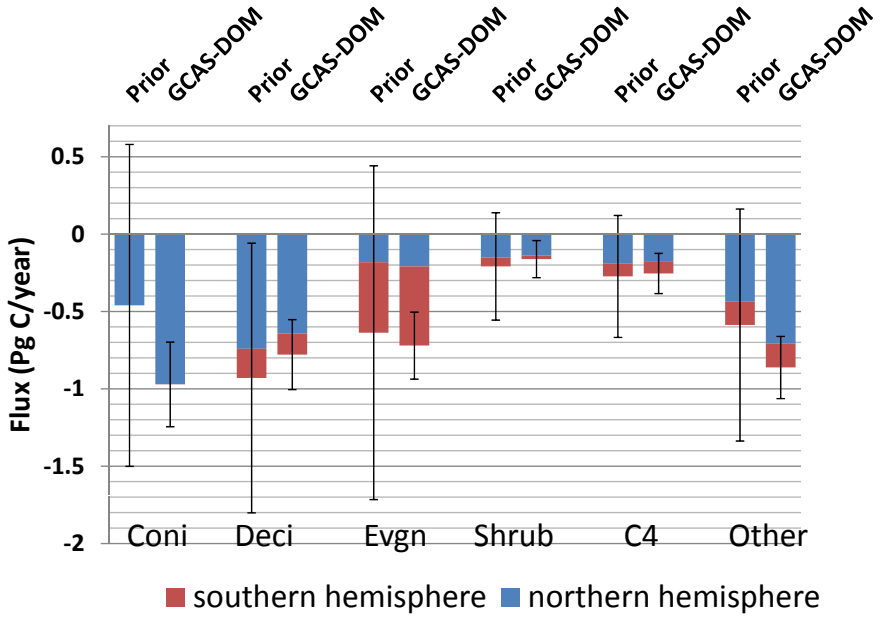

Figure 7. Annual mean flux per PFT and its uncertainty for the period ~~2000–2007~~2001–2007. Coni stands for coniferous forest, Deci for deciduous forest, Evgn for evergreen forest, Shrub for shrub land, C4 for C4 vegetation and Other for other vegetation. "Prior", "GCAS-DOM" are the fluxes before and after optimization. All units are in $\mathrm{Pg\,C\,year^{-1}}$.

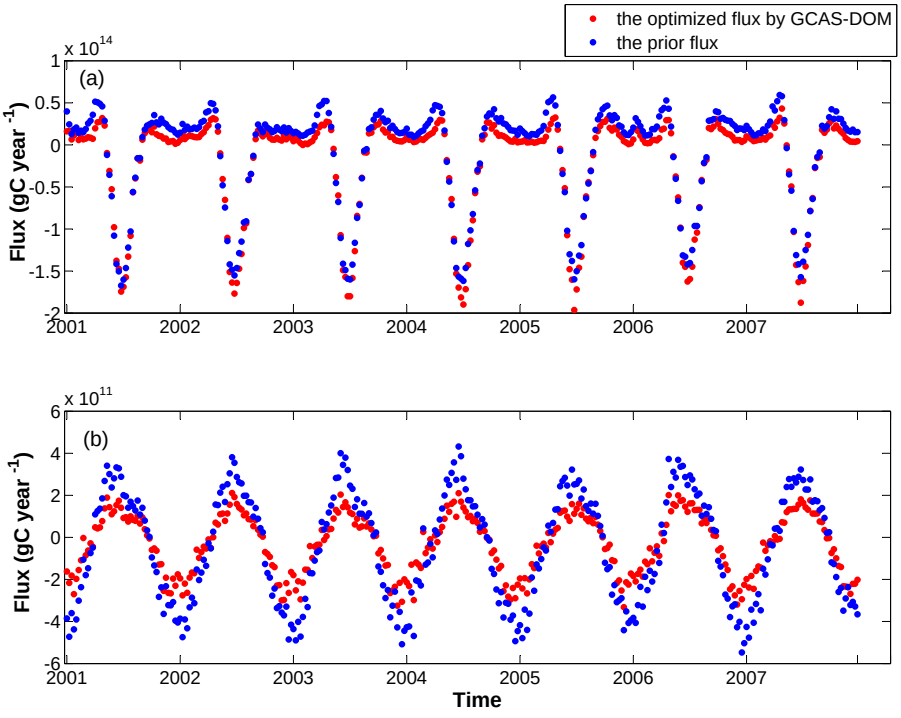

Figure 8. Weekly fluxes for coniferous forest. **(a)** Northern Hemisphere **(b)** Southern Hemisphere. All units are in $\mathrm{g\,C\,year^{-1}}$. Note different scales are used.

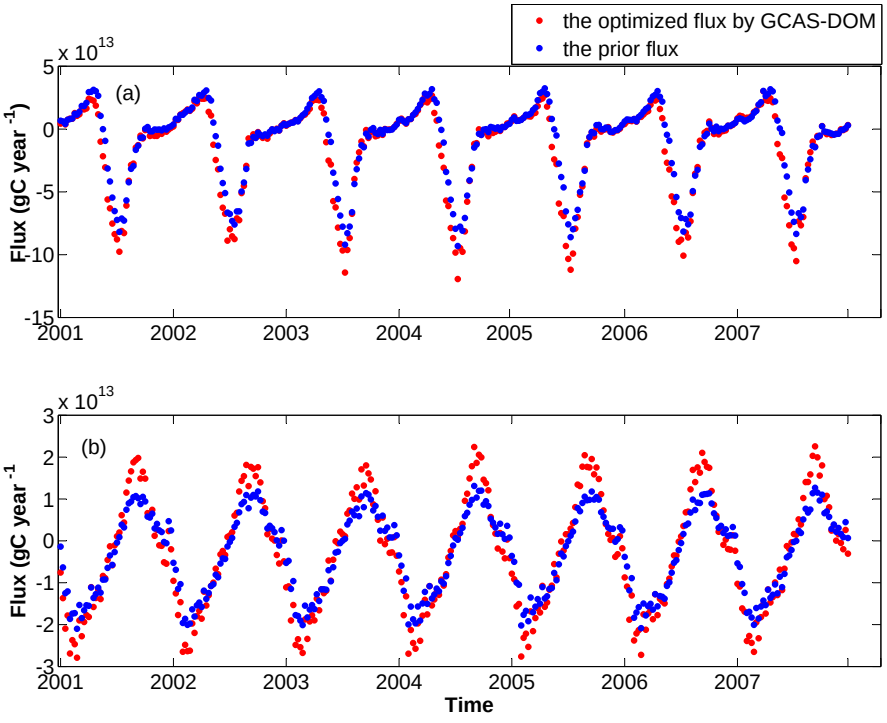

Figure 9. Weekly fluxes for "other vegetation". **(a)** Northern Hemisphere **(b)** Southern Hemisphere. All units are in $\mathrm{g\,C\,year^{-1}}$. Note different scales are used.

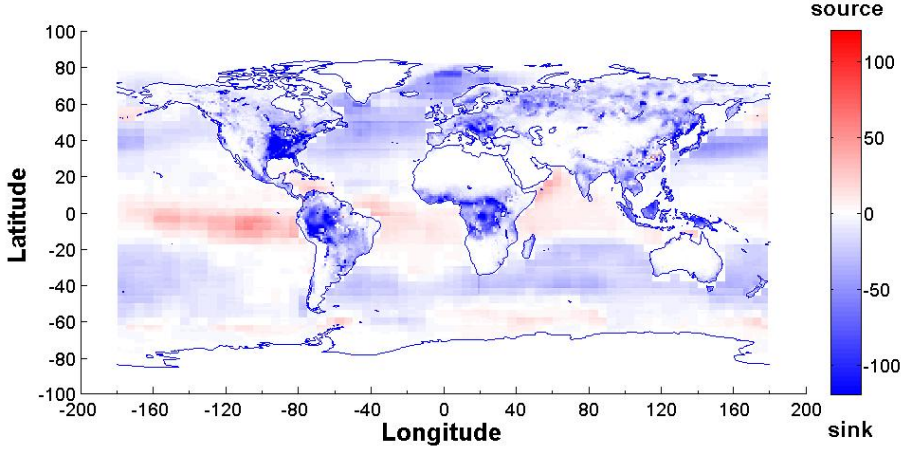

Figure 10. The average annual pattern of the prior flux for the years ~~2000–2007~~ 2001–2007 excluding fossil fuel and fire emissions (in $\mathrm{g\,C\,m^{-2}\,year^{-1}}$).

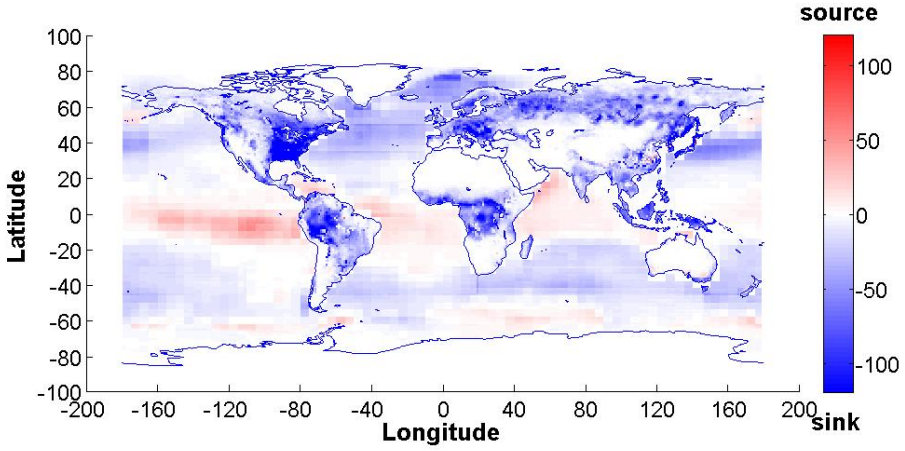

Figure 11. The average annual pattern of the optimized flux by GCAS-DOM for the years ~~2000–2007~~ 2001–2007 (in g C m^{-2} $year^{-1}$).

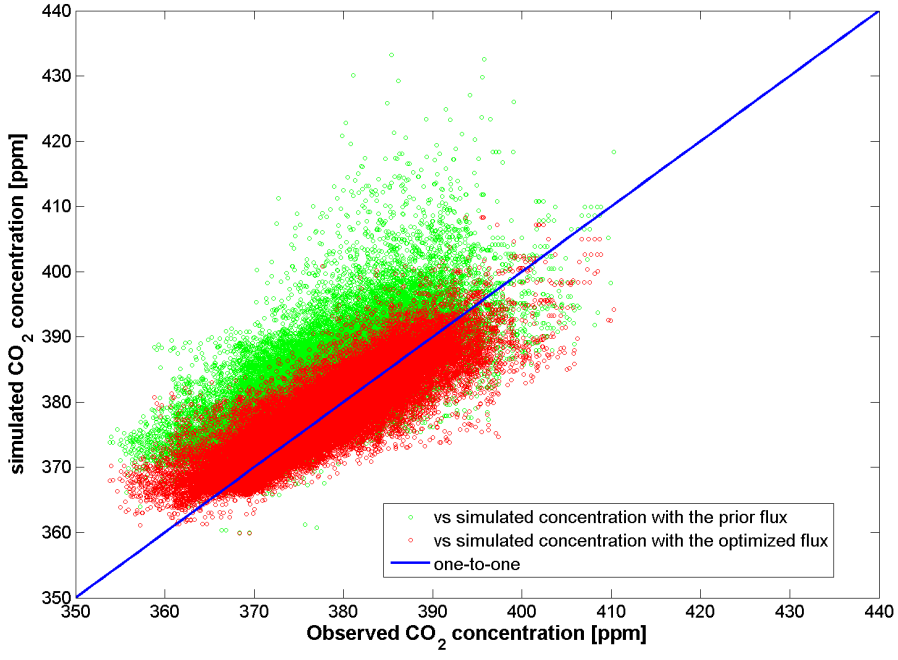

Figure 12. Comparison between observed concentration with simulated concentration.

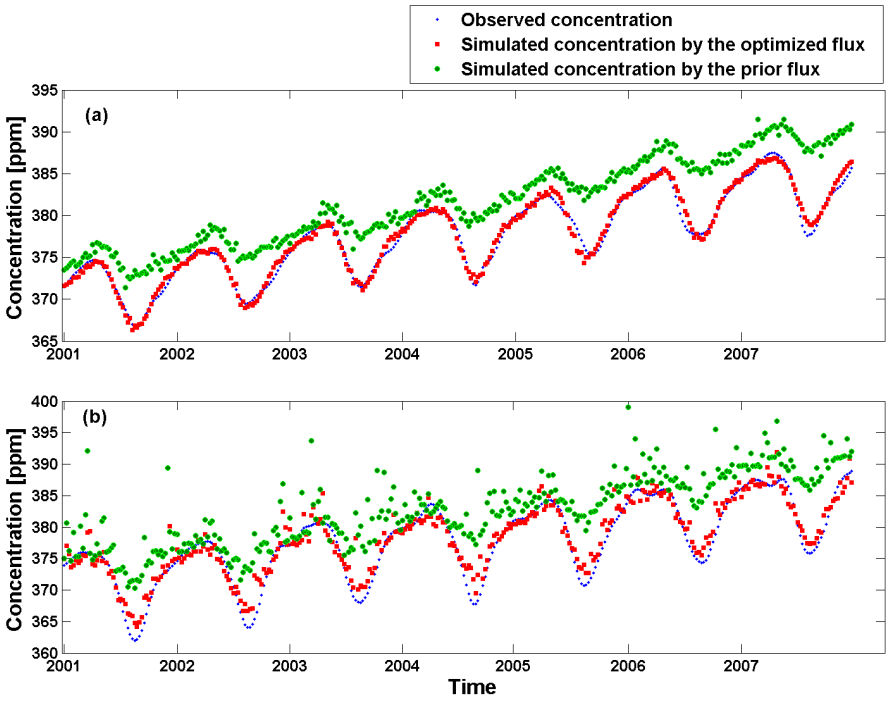

Figure 13. Observed (blue dot) concentration, simulated concentration with the optimized flux (red square) and simulated concentration with the prior flux (green circle) from **(a)** Dahlen, North Dakota, United States (47.5° N 99.24° W) **(b)** Mace Head, County Galway, Ireland (53.33° N, 9.9° W).

Figure 14. Simulated-minus-observed CO_2 for a set of 312 observation sites by week.